

1 High-resolution genetic mapping of the 2 mucosa-associated gut microbiome in hybrid 3 mice provides novel insight on the impact of 4 host genetics

5 Shauni Doms^{1,2}, Hanna Fokt^{1,2}, Malte Christoph Rühlemann^{3,4}, Cecilia J. Chung^{1,2},
6 Axel Künstner⁵, Saleh Ibrahim⁵, Andre Franke³, Leslie M. Turner^{7**†} and John F.
7 Baines^{1,2*†}

8 ¹ Max Planck Institute for Evolutionary Biology, Plön, Germany

9 ² Section of Evolutionary Medicine, Institute for Experimental Medicine, Kiel University, Kiel,
10 Germany

11 ³ Institute for Clinical Molecular Biology (IKMB), Kiel University, Kiel Germany

12 ⁴ Institute for Medical Microbiology and Hospital Epidemiology, Hannover Medical School,
13 Hannover, Germany

14 ⁵ Institute of Experimental Dermatology, University of Lübeck, Lübeck, Germany

15 ⁶ Sharjah Institute of Medical Research, Sharjah, UAE

16 ⁷ Milner Centre for Evolution, Department of Biology & Biochemistry, University of Bath,
17 United Kingdom

18 * Correspondence: l.m.turner@bath.ac.uk; baines@evolbio.mpg.de

19 † These authors contributed equally to this work.

20 **Abstract:** Determining the forces that shape diversity in host-associated bacterial
21 communities is critical to understanding the evolution and maintenance of meta-
22 organisms. To gain novel insight on the genetics of gut microbial traits, we employed a
23 powerful approach using inbred lines derived from the hybrid zone of two incipient
24 house mouse species and uniquely investigated the microbiome at the gut mucosal
25 interface. We identify a high number of mucosa-associated bacterial taxa with significant
26 heritability estimates, particularly for 16S rRNA transcript-based traits. Interestingly,
27 heritability estimates also positively correlate with cospeciation rate estimates.
28 Association mapping identifies 443 loci influencing 123 taxa, whose narrow genomic
29 intervals enable promising individual candidate genes and pathways to be pinpointed.
30 These results indicate a unique genetic architecture for cospeciating taxa, a clear
31 enrichment for several classes of human disease, including inflammatory bowel disease,
32 and identify important functional categories including innate immunity and G-protein-
33 coupled receptors, whose role in host-microbe interactions diverge as new species form.

34 **Keywords:** microbiome; GWAS; cospeciation; codiversification; hybridization;
35 phylosymbiosis

36 Introduction

37 The recent widespread recognition of the gut microbiome's importance to host
38 health and fitness represents a critical advancement of biomedicine. Host phenotypes
39 affected by the gut microbiome are documented in humans (Ley et al., 2006; Turnbaugh
40 et al., 2009; Lynch and Pedersen, 2016), laboratory animals (Backhed et al., 2004;
41 Turnbaugh et al., 2008; Rolig et al., 2015; Rosshart et al., 2017; Gould et al., 2018), and
42 wild populations (Suzuki, 2017; Roth et al., 2019; Suzuki et al., 2020; Hua et al., 2020),
43 and include critical traits such as aiding digestion and energy uptake (Rowland et al.,
44 2018), and the development and regulation of the immune system (Davenport, 2020).

45 Despite the importance of gut microbiome, community composition varies
46 significantly among host species, populations, and individuals (Benson et al., 2010;
47 Yatsunencko et al., 2012; Brooks et al., 2016; Rehman et al., 2016; Amato et al., 2019).
48 While a portion of this variation is expected to be selectively neutral, alterations of the
49 gut microbiome are on the one hand linked to numerous human diseases (Carding et al.,
50 2015; Lynch and Pedersen, 2016) such as diabetes (Qin et al., 2012), inflammatory bowel
51 disease (IBD) (Ott et al., 2004; Gevers et al., 2014) and mental disorders (Clapp et al.,
52 2017). On the other hand, there is evidence that the gut microbiome can play an
53 important role in adaptation on both recent- (Hehemann et al., 2010; Suzuki and Ley,
54 2020) and ancient evolutionary timescales (Rausch et al., 2019). Collectively, these
55 phenomena suggest that it would be evolutionarily advantageous for hosts to influence
56 their microbiome.

57 An intriguing observation made in comparative microbiome research in the last
58 decade is that the pattern of diversification among gut microbiomes appears to mirror
59 host phylogeny (Ochman et al., 2010). This phenomenon, coined "phylosymbiosis"
60 (Brucker and Bordenstein, 2012a; Brucker and Bordenstein, 2012b; Lim and Bordenstein,
61 2020), is documented in a number of diverse host taxa (Brooks et al., 2016) and also
62 extends to the level of the phageome (Gogarten et al., 2021). Several non-mutually
63 exclusive hypotheses are proposed to explain phylosymbiosis (Moran and Sloan, 2015).
64 However, it is likely that vertical inheritance is important for at least a subset of taxa, as
65 signatures of co-speciation/-diversification are present among numerous mammalian
66 associated gut microbes (Moeller et al., 2016; Groussin et al., 2017; Moeller et al., 2019),
67 which could also set the stage for potential coevolutionary processes. Importantly,
68 experiments involving interspecific fecal microbiota transplants indeed provide
69 evidence of host adaptation to their conspecific microbial communities (Brooks et al.,
70 2016; Moeller et al., 2019). Further, cospeciating taxa were observed to be significantly
71 enriched among the bacterial species depleted in early onset IBD, an immune-related
72 disorder, suggesting a greater evolved dependency on such taxa (Papa et al., 2012;
73 Groussin et al., 2017). However, the nature of genetic changes involving host-microbe
74 interactions that take place as new host species diverge remains under-explored.

75 House mice are an excellent model system for evolutionary microbiome research, as

76 studies of both natural populations and laboratory experiments are possible (Suzuki,
77 2017; Suzuki et al., 2019). In particular, the house mouse species complex is comprised of
78 subspecies that hybridize in nature, enabling the potential early stages of
79 codiversification to be studied. We previously analyzed the gut microbiome across the
80 central European hybrid zone of *Mus musculus musculus* and *M. m. domesticus* (Wang et
81 al., 2015), which share a common ancestor ~ 0.5 million years ago (Geraldès et al., 2008).
82 Importantly, transgressive phenotypes (i.e. exceeding or falling short of parental values)
83 among gut microbial traits as well as increased intestinal histopathology scores were
84 common in hybrids, suggesting that the genetic basis of host control over microbes has
85 diverged (Wang et al., 2015). The same study performed an F₂ cross between wild-
86 derived inbred strains of *M. m. domesticus* and *M. m. musculus* and identified 14
87 quantitative trait loci (QTL) influencing 29 microbial traits. However, like classical
88 laboratory mice, these strains had a history of rederivation and reconstitution of their
89 gut microbiome, thus leading to deviations from the native microbial populations found
90 in nature (Rosshart et al., 2017; Org and Lusiš, 2018), and the genomic intervals were too
91 large to identify individual genes.

92 In this study, we employed a powerful genetic mapping approach using inbred
93 lines directly derived from the *M. m. musculus* - *M. m. domesticus* hybrid zone, and
94 further focus on the mucosa-associated microbiota due to its more direct interaction
95 with host cells (Fukata and Arditi, 2013; Chu and Mazmanian, 2013), distinct functions
96 compared to the luminal microbiota (Wang et al., 2010; Vaga et al., 2020), and greater
97 dependence on host genetics (Spor et al., 2011; Linnenbrink et al., 2013). Previous
98 mapping studies using hybrids raised in a laboratory environment showed that high
99 mapping resolution is possible due to the hundreds of generations of natural admixture
100 between parental genomes in the hybrid zone (Turner and Harr, 2014; Pallares et al.,
101 2014; Škrabar et al., 2018). Accordingly, we here identify 443 loci contributing to
102 variation in 123 taxa, whose narrow genomic intervals (median <2Mb) enable many
103 individual candidate genes and pathways to be pinpointed. We identify a high
104 proportion of bacterial taxa with significant heritability estimates, and find that bacterial
105 phenotyping based on 16S rRNA transcript compared to gene copy-based profiling
106 yields an even higher proportion. Further, these heritability estimates also significantly
107 positively correlate with cospeciation rate estimates, suggesting a more extensive host
108 genetic architecture for cospeciating taxa. Finally, we identify numerous enriched
109 functional pathways, whose role in host-microbe interactions may be particularly
110 important as new species form.

111 Results

112 *Microbial community composition*

113 To obtain microbial traits for genetic mapping in the G2 mapping population, we
114 sequenced the 16S rRNA gene from caecal mucosa samples of 320 hybrid male mice
115 based on DNA and RNA (cDNA), which reflect bacterial cell number and activity,
116 respectively. After applying quality filtering and subsampling 10,000 reads per sample,
117 we identified a total of 4684 amplicon sequence variants (ASVs). For further analyses,
118 we established a "core microbiome" (defined in Methods), such that analyses were
119 limited to those taxa common and abundant enough to reveal potential genetic signal.
120 The core microbiome is composed of four phyla, five classes, five orders, eleven families,
121 27 genera, and 90 ASVs for RNA, and four phyla, five classes, six orders, twelve families,
122 28 genera and 46 ASVs for DNA. A combined total of 98 unique ASVs belong to the core,
123 of which 38 were shared between DNA and RNA (Suppl. Fig. 1). The most abundant
124 genus in our core microbiome is *Helicobacter* (Suppl. Fig. 2), consistent with a previous
125 study of the wild hybrid *M. m. musculus*/*M. m. domesticus* mucosa-associated
126 microbiome (Wang et al., 2015).

127 *Correlation between host genetic relatedness and microbiome structure*

128 To gain a broad sense of the contribution of genetic factors to the variability of
129 microbial phenotypes in our mapping population, we compared the kinship matrix
130 based on genotypes to an equivalent based on gut microbial composition, whereby ASV
131 abundances were used as equivalents of gene dosage. We found a significant correlation
132 between these matrices ($P = .001$; Suppl. Fig. 3), indicating a host genetic effect on the
133 diversity of the gut microbiota.

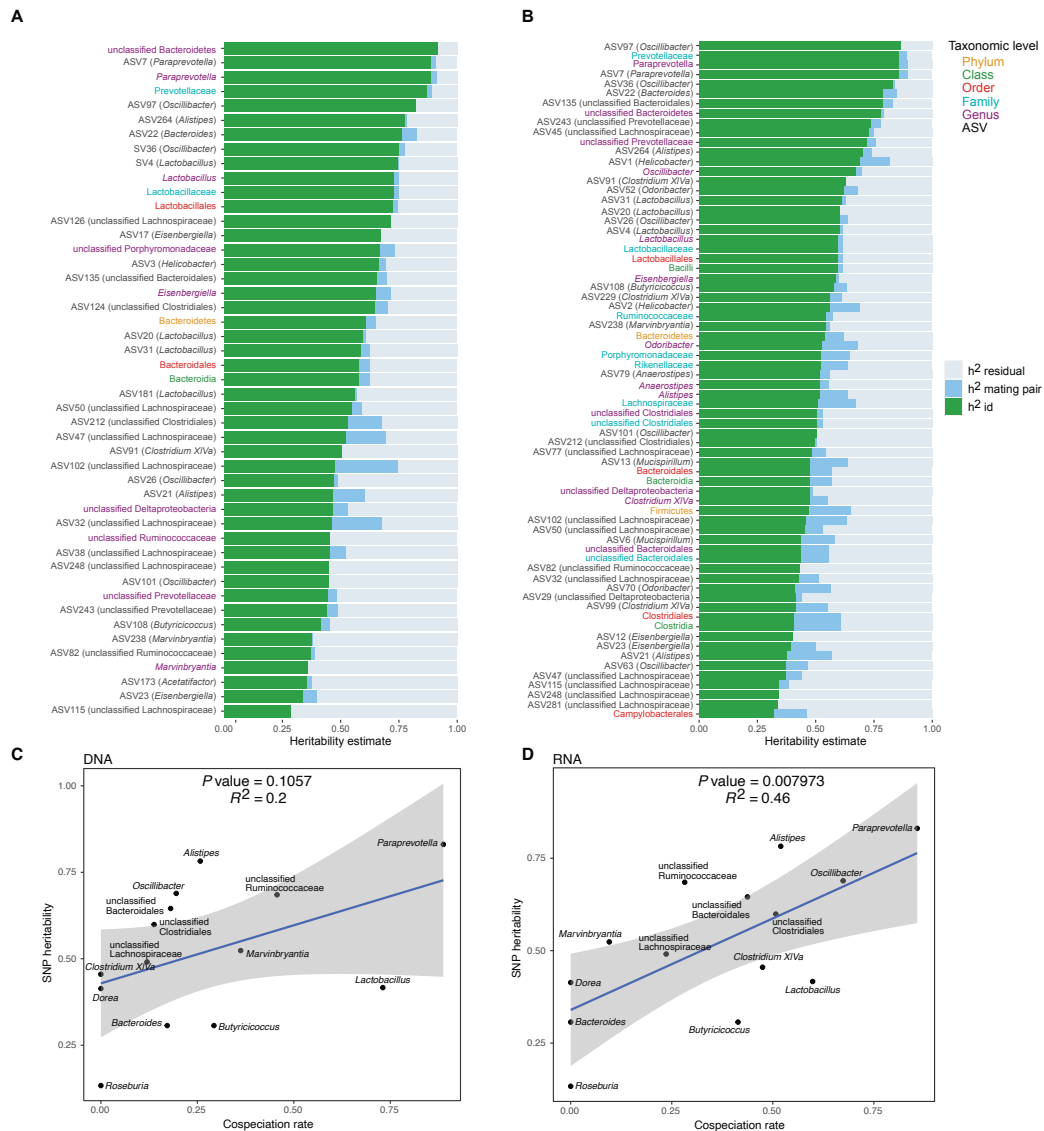
134 *SNP-based heritability*

135 Next, we used a SNP-based approach to estimate the proportion of variance
136 explained (PVE) of the relative abundance of taxa, also called the narrow-sense
137 heritability (h^2) or SNP-based heritability. Out of the 153 total core taxa, we identified 46
138 taxa for DNA and 69 taxa for RNA with significant heritability estimates ($P_{RLRT} < .05$),
139 with estimates ranging between 29 and 91% (see Fig. 1A-B and Suppl. Table 1). An
140 unclassified genus belonging to the phylum Bacteroidetes followed by ASV7 (genus
141 *Paraprevotella*), *Paraprevotella* and Paraprevotellaceae showed the highest heritability
142 among DNA-based traits (91.8%, 88.8%, 88.8%, and 87.1%, respectively; Fig. 1A), while
143 ASV97 (genus *Oscillibacter*), followed by Prevotellaceae, *Paraprevotella* and ASV7
144 (*Paraprevotella*) had the highest heritability among RNA-based traits (86.6%, 85.7%,
145 85.7%, and 85.6%, resp.; Fig. 1B). The heritability estimates for DNA- and RNA-based
146 measurements of the same taxa are significantly correlated ($P = 5.013 \times 10^{-8}$, $R^2=0.58$,
147 Suppl. Fig. 4), and neither measure appears to be systematically more heritable than

148 another, i.e. some taxa display higher RNA-based heritability estimates and others
 149 higher DNA-based estimates.

150 *Heritability estimates are correlated with predicted co-speciation rates*

151 In an important meta-analysis of the gut microbiome across diverse mammalian
 152 taxa, Groussin et al. (2017) estimated co-speciation rates of individual bacterial taxa by
 153 measuring the congruence of host and bacteria phylogenetic trees relative to the number
 154 of host-swap events. We reasoned that taxa with higher co-speciation rates might also
 155 demonstrate higher heritability, as these more intimate evolutionary relationships would
 156 provide a greater opportunity for genetic aspects to evolve. Intriguingly, we observe a
 157 significant positive correlation for RNA-based traits ($P = .008$, $R^2 = .46$, Fig. 1D) and a
 158 similar trend for DNA ($P = 0.1$; Fig. 1C). These results support the notion that
 159 cospeciating taxa evolved a greater dependency on host genes, and further suggest that
 160 bacterial activity may better reflect the underlying biological interactions.

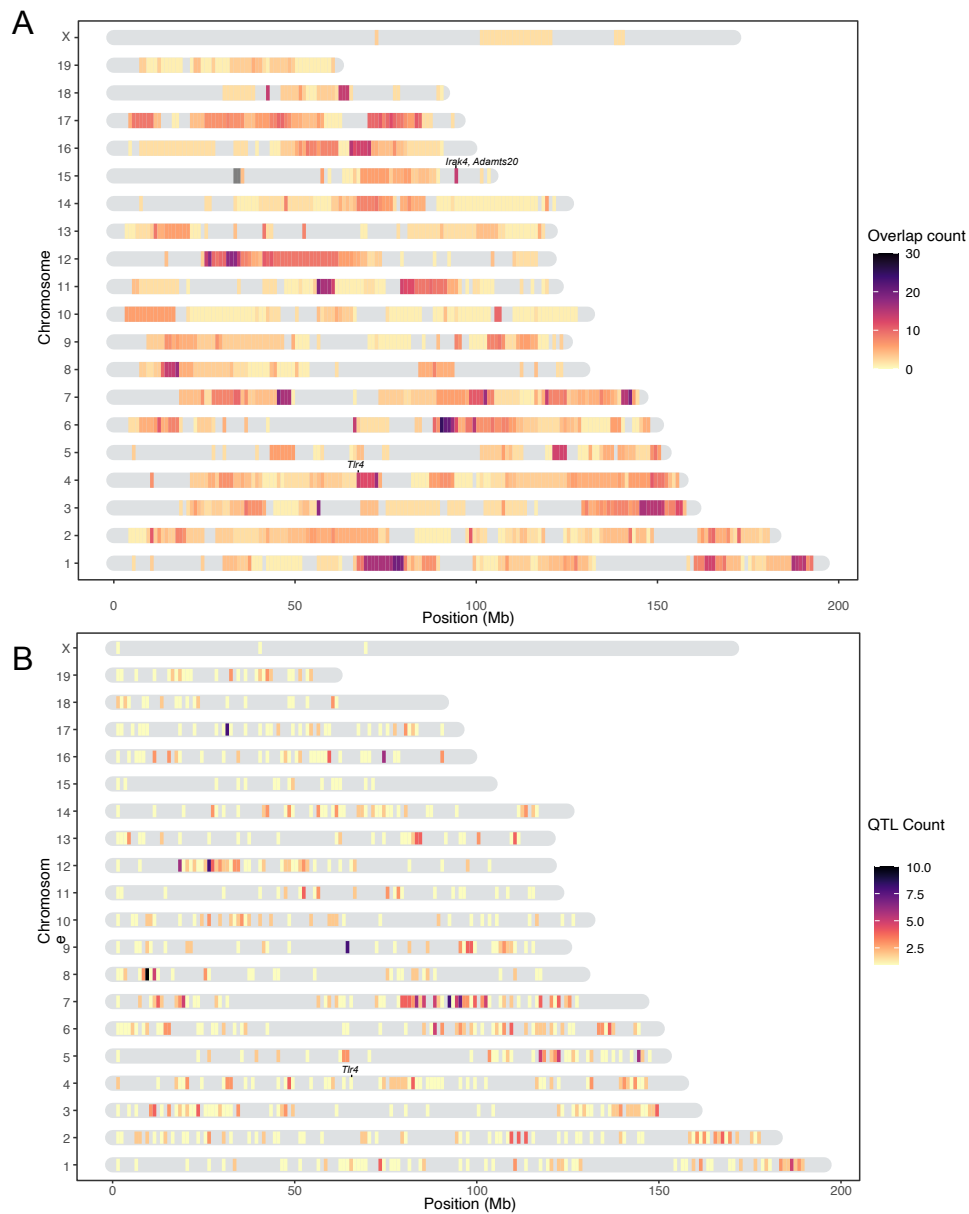


161 **Figure 1:** (A-B) Heritability estimates for the relative abundance of bacterial taxa. Proportion
162 of variance explained for each taxon on DNA level (A), and RNA level (B) for all SNPs (GRM) in
163 green, mating pair identifier in blue and residual variance in grey. Only significant heritability
164 estimates are shown ($P < .05$). The text labels on the y-axis are colored according to taxonomic
165 level: ASV in black, genus in purple, family in light blue, order in red, class in green, and phylum
166 in yellow. (C-D) Relationship between the heritability estimates for the relative abundance of
167 bacterial taxa and co-speciation rate for the same genus calculated by Groussin et al. (2017). DNA
168 level (C), and RNA level (D). The blue line represents a linear regression fit to the data and the
169 grey area the corresponding confidence interval.

170 *Genetic mapping of host loci determining microbiome composition*

171 Next, we performed genome-wide association mapping of the relative abundances
172 of core taxa, in addition to two alpha-diversity measures (Shannon and Chao1 indices),
173 based on 32,625 SNPs. We included both additive and dominance terms in the model to
174 enable the identification of under- and over-dominance (see Methods). While we found
175 no significant associations for alpha diversity at either the DNA or RNA level ($P > 1.53 \times$
176 10^{-6}), a total of 1099 genome-wide significant associations were identified for individual
177 taxa ($P < 1.53 \times 10^{-6}$, Suppl. Table 2), of which 443 achieved study-wide significance (P
178 $< 1.29 \times 10^{-8}$). Apart from the X chromosome, all autosomal chromosomes contained
179 study-wide significant associations (Fig. 2). Out of the 153 mapped taxa, 123 had at least
180 one significant association (Table 1). For the remainder of our analyses, we focus on the
181 results using the more stringent study-wide threshold, and combined significant SNPs
182 within 10 Mb into significant regions (Suppl. Table 3). The median size of significant
183 regions is 1.91 Mb, which harbor a median of 14 protein-coding genes. On average, we
184 observe 10 significant mouse genomic regions per bacterial taxon.

185 Of the significant loci with estimated interval sizes, we find 73 intervals (16.5%) that
186 are smaller than one Mb (Suppl. Table 4). The smallest interval is only 231 bases and
187 associated with the RNA-based abundance of an unclassified genus belonging to
188 Deltaproteobacteria. It is situated in an intron of the C3 gene, a complement component
189 playing a central role in the activation of the complement system, which modulates
190 inflammation and contributes to antimicrobial activity (Ricklin et al., 2016).



191 Figure 2: Heatmap of significant host loci from association mapping of bacterial
192 abundances. Karotype plot showing the number of significant loci found using a study-
193 wide threshold, where (A) plots the significance intervals, and (B) the significant SNP
194 markers on the chromosomes.

195 Table. 1. Overview of mapping statistics.

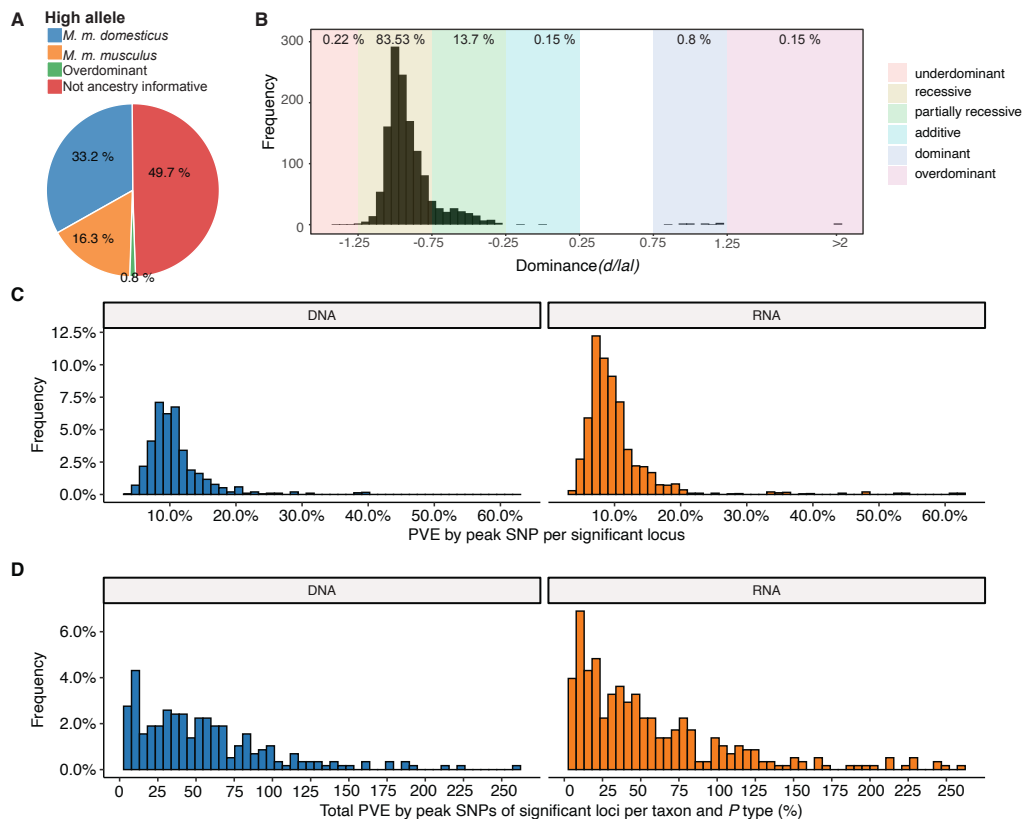
196		DNA	RNA	Total
197	Mapped taxa	101	142	153
198	Taxa with significant loci	67	96	123
199	Median interval size (Mb)	1.52	2.29	1.91
200	Total significant loci	478	791	1269
201	Unique significant loci	179	313	443
202	Significant loci total P	91	167	233
203	Significant loci additive P	155	260	377
204	Significant loci dominance P	95	166	231
205	Median significant loci per trait	5	6	8
206	Median unique significant loci per trait	3	3	4
207	Median unique significant SNPs per locus	2	2.5	2
208	Median number of genes per locus	31	52	43
209	Median protein coding genes per locus	11	15	14

210 The significant genomic regions and SNPs are displayed in Figure 2A and 2B,
211 respectively. Individual SNPs were associated with up to 12 taxa, and significant
212 intervals with up to 30 taxa. The SNPs with the lowest P values were associated with the
213 genus *Dorea* and two ASVs belonging to *Dorea* (ASV184 and ASV293; Suppl. Fig. 5). At
214 the RNA level this involves two loci: mm10-chr4: 67.07 Mb, where the peak SNP is 13 kb
215 downstream of the closest gene *Tlr4* (UNC7414459, $P=2.31 \times 10^{-69}$, additive $P= 4.48 \times$
216 10^{-118} , dominance $P= 1.37 \times 10^{-111}$), and mm10-chr15: 94.4 Mb, where the peak SNP is
217 found within the *Adamts20* gene (UNC26145702, $P=4.51 \times 10^{-65}$, additive $P= 1.87 \times 10^{-113}$,
218 dominance $P= 1.56 \times 10^{-105}$; Fig. 2; Suppl. Fig. 5). Interestingly, the *Irak4* gene, whose
219 protein product is rapidly recruited after TLR4 activation, is also located 181 kb
220 upstream of *Adamts20*. The five taxa displaying the most associations were ASV19
221 (*Bacteroides*), *Dorea*, ASV36 (*Oscillibacter*), ASV35 (*Bacteroides*), and ASV98 (unclassified
222 Lachnospiraceae) (Suppl. Fig. 6).

223 *Ancestry, dominance, and effect sizes*

224 A total of 435 significant SNPs were ancestry informative between *M. m. musculus*
225 and *M. m. domesticus* (*i.e.* represent fixed differences between subspecies). To gain further
226 insight on the genetic architecture of microbial trait abundances, we estimated the
227 degree of dominance at each significant locus using the
228 d/a ratio (Falconer, 1996), where alleles with strictly recessive, additive, and dominant
229 effects have d/a values of -1, 0, and 1, respectively. As half of the SNPs were not ancestry
230 informative (Fig. 3A), it was not possible to consistently have a associated with one
231 parent/subspecies, hence we report $d/|a|$ such that it can be interpreted with respect to
232 bacterial abundance. For the vast majority of loci (83.53%), the allele associated with
233 lower abundance is dominant or partially dominant ($-1.25 < d/|a| < -0.75$; Fig. 3B). On
234 the basis of the arbitrary cutoffs we used to classify dominance, only a small proportion

235 of alleles are underdominant (0.22%; $d/|a| < -1.25$) or overdominant (0.15%; $d/|a| >$
 236 1.25). However for one-third of the significant SNPs, the heterozygotes display
 237 transgressive phenotypes, i.e. mean abundances that are either significantly lower (31%
 238 of SNPs)- or higher (2% of SNPs) than those of both homozygous genotypes.
 239 Interestingly, the *domesticus* allele was associated with higher bacterial abundance in
 240 two-thirds of this subset (33.2% vs 16.3% *musculus* allele; Fig. 3A).



241 **Figure 3:** Genetic architecture of significant loci. A) Source of the allele with the highest phenotypic value. B) Histogram of dominance values d/a of significant loci reveals a majority of loci acting recessive or partially recessive. C) Histogram showing the percentage of variance explained (PVE) by the peak SNP for DNA (blue, left) and RNA (orange, right). D) Collective PVE by lead SNPs of significant loci within a taxon. Values are calculated separately for each P value type (total, additive, and dominance).

247 Next, we estimated phenotypic effect sizes by calculating the percentage variance
 248 explained (PVE) by the peak SNP of each significant region. Peak SNPs explain between
 249 3% and 64% of the variance in bacterial abundance, with a median effect size of 9.3%
 250 (Fig. 3C). The combined effects of all significant loci for each taxon ranged from 4.9% to
 251 259%, with a median of 41.8% (Fig. 3D). Note, combined effects for many taxa (33 out of
 252 59) exceed SNP-heritability estimates (Fig. 1). While exceeding 100% explained variance
 253 is biologically possible, as loci can have opposite phenotypic effects, many of these are
 254 likely inflated due to the Beavis effect (Beavis, 1994).

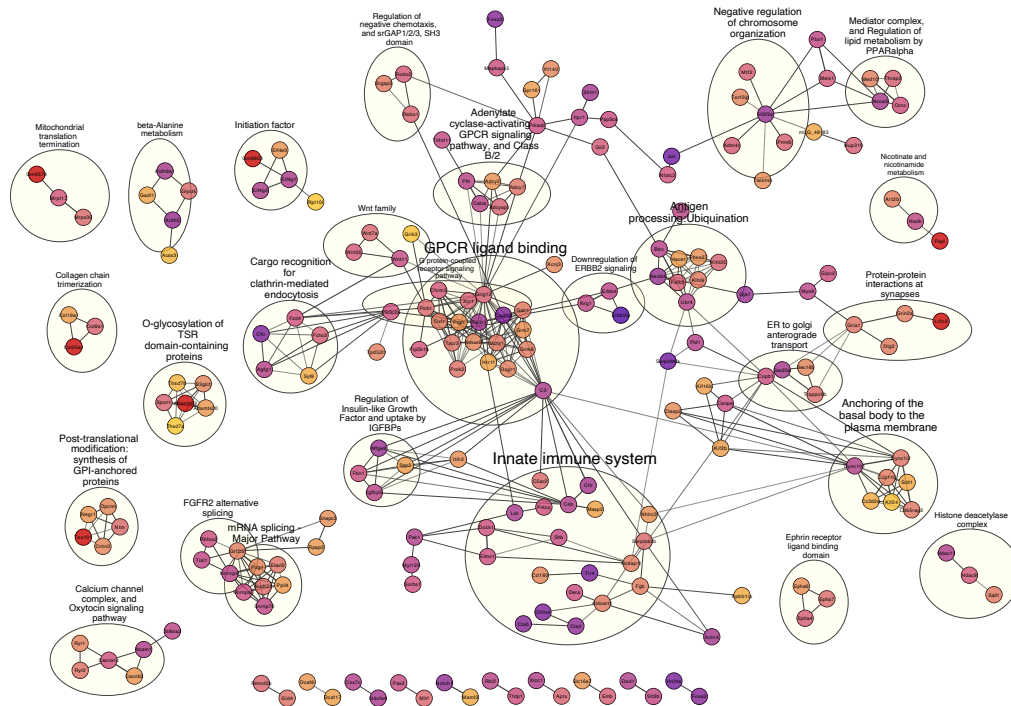
255 *Functional annotation of candidate genes*

256 In order to reveal potential higher level biological phenomena among the identified
257 loci, we performed pathway analysis to identify interactions and functional categories
258 enriched among the genes in significant intervals. We used STRING (Szklarczyk et al.,
259 2019) to calculate a protein-protein interaction (PPI) network of 925 protein-coding
260 genes nearest to significant SNPs (upstream and/or downstream). A total of 768 genes
261 were represented in the STRING database, and the maximal network is highly
262 significant (PPI enrichment P value: 2.15×10^{-14}) displaying 668 nodes connected by 1797
263 edges and an average node degree of 4.68. After retaining only the edges with the
264 highest confidence (interaction score > 0.9), this results in one large network with 233
265 nodes, 692 edges and ten smaller networks (Fig. 4).

266 Next, we functionally annotated clusters using STRING's functional enrichment
267 plugin. The genes of the largest cluster are part of the G protein-coupled receptor
268 (GPCR) ligand binding pathway. GPCRs are the largest receptor superfamily and also
269 the largest class of drug targets (Sriram and Insel, 2018). We then calculated the top ten
270 hub proteins from the network based on Maximal Clique Centrality (MCC) algorithm
271 with CytoHubba to predict important nodes that can function as 'master switches'
272 (Suppl. Fig. 7). The top ten proteins contributing to the PPI network were GNG12,
273 MCHR1, NMUR2, PROK2, OXTR, XCR1, TACR3, CHRM3, PTGFR, and C3, which are
274 all involved in the GPCR signaling pathway.

275 Further, we performed enrichment analysis on the 925 genes nearest to significant
276 SNPs using the *clusterprofiler* R package. We found 14 KEGG pathways to be over-
277 represented: circadian entrainment, oxytocin signaling pathway, axon guidance, calcium
278 signaling, cAMP signaling, cortisol synthesis and secretion, cushing syndrome, gastric
279 acid secretion, glutamatergic synapse, mucin type O-glycan biosynthesis, inflammatory
280 mediator regulation of TRP channels, PD-L1 expression and the PD-1 checkpoint
281 pathway in cancer, tight junction, and the *Wnt* signaling pathway (Suppl. Table 5, Suppl.
282 Fig. 8-9). Finally, genes involved in five human diseases are enriched, among them
283 mental disorders (Suppl. Fig. 10).

284 Finally, due to the observation of a significant enrichment of cospeciating taxa
285 among the bacterial species depleted in early onset IBD (Groussin et al., 2017) and the
286 evidence that IBD is especially associated with a dysbiosis in mucosa-associated
287 communities (Yang et al., 2020a; Daniel et al., 2021), we specifically examined possible
288 over-representation of genes involved in IBD (Khan et al., 2021) among the 925 genes
289 neighboring significant SNPs. We found 14 out of the 289 IBD genes, which was
290 significantly more than expected by chance (10 000 times permuted mean: 2.7, simulated
291 $P = .0001$; Suppl. Table 6). Interestingly, SNPs in five out of the 14 genes are associated
292 with ASVs belonging to the genus *Oscillibacter*, a cospeciating taxon known to decrease
293 during the active state of IBD (Metwaly et al., 2020).



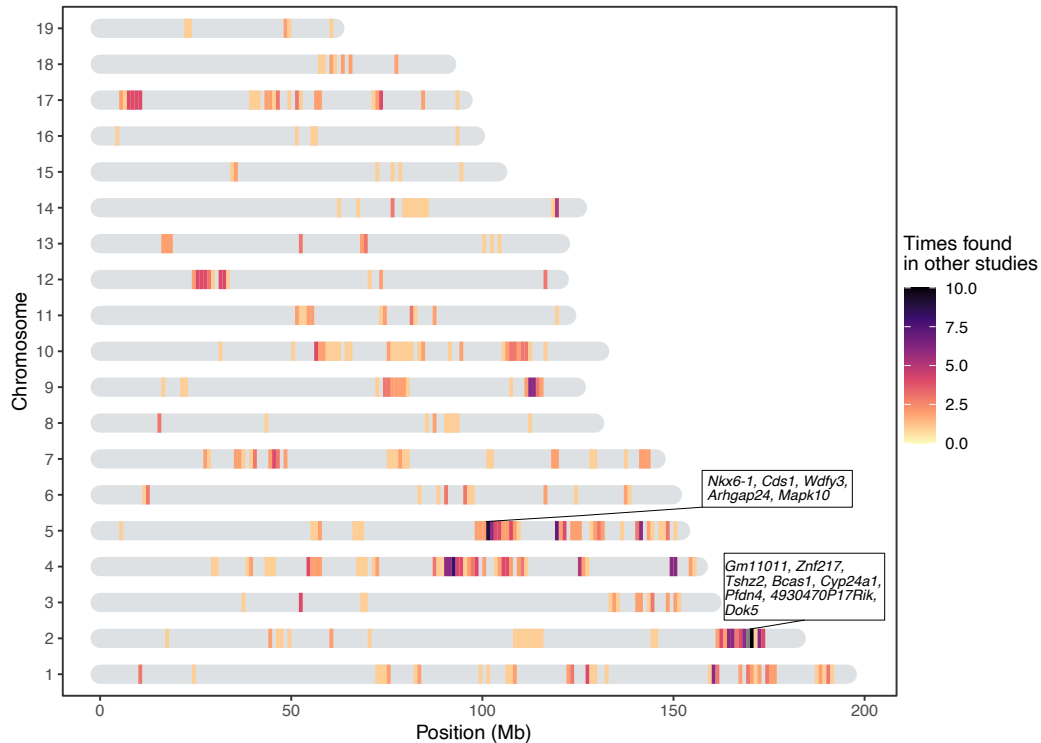
294 **Figure 4:** High confidence protein-protein interaction network of genes closest to SNPs
295 significantly associated with bacterial abundances. Network clusters are annotated using
296 STRING's functional enrichment (Doncheva et al., 2019). Nodes represent proteins and
297 edges their respective interactions. Only edges with an interaction score higher than 0.9
298 are retained. The width of the edge line expresses the interaction score calculated by
299 STRING. The color of the nodes describe the expression of the protein in the intestine
300 where yellow is not expressed and purple is highly expressed.

301 *Comparison of significant loci to published gut microbiome mapping studies*

302 Next, we compiled a list of 648 unique confidence intervals of significant
303 associations with gut bacterial taxa from seven previous mouse QTL studies (Benson et
304 al., 2010; McKnite et al., 2012; Leamy et al., 2014; Wang et al., 2015; Org et al., 2015;
305 Snijders et al., 2016; Kemis et al., 2019) and compared this list to our significance
306 intervals for bacterial taxa at both the DNA and RNA level (346 unique intervals).
307 Regions larger than 10Mb were removed from all studies. We found 434 overlapping
308 intervals, which is significantly more than expected by chance (10 000 times permuted
309 mean: 368, simulated $P=0.0073$, see Methods). Several of our smaller significant loci
310 overlapped with larger loci from previous studies and removing this redundancy left
311 186 significant loci with a median interval size of 0.78 Mb (Fig. 5). The most frequently
312 identified locus is located on chromosome 2 169-171 Mb where protein coding genes
313 *Gm11011*, *Znf217*, *Tshz2*, *Bcas1*, *Cyp24a1*, *Pfdn4*, *4930470P17Rik*, and *Dok5* are situated.

314 Additionally, we collected genes within genome-wide significant regions reported
315 in seven human microbiome GWAS (mGWAS) (Bonder et al., 2016; Turpin et al., 2016;

316 Goodrich et al., 2016; Wang et al., 2016; Hughes et al., 2020; Rühlemann et al., 2021;
317 Kurilshikov et al., 2021). However, no significant over-representation of genes was
318 found within our significance intervals ($P = .156$), nor within our list of genes closest to a
319 significant SNP ($P = .62$).



320 **Figure 5:** Heatmap showing the significant loci in this study that were previously
321 found in other QTL studies of the mouse gut microbiome. The genes present in
322 two repeatedly identified regions are depicted in boxes.

323 *Proteins differentially expressed in germ-free vs conventional mice*

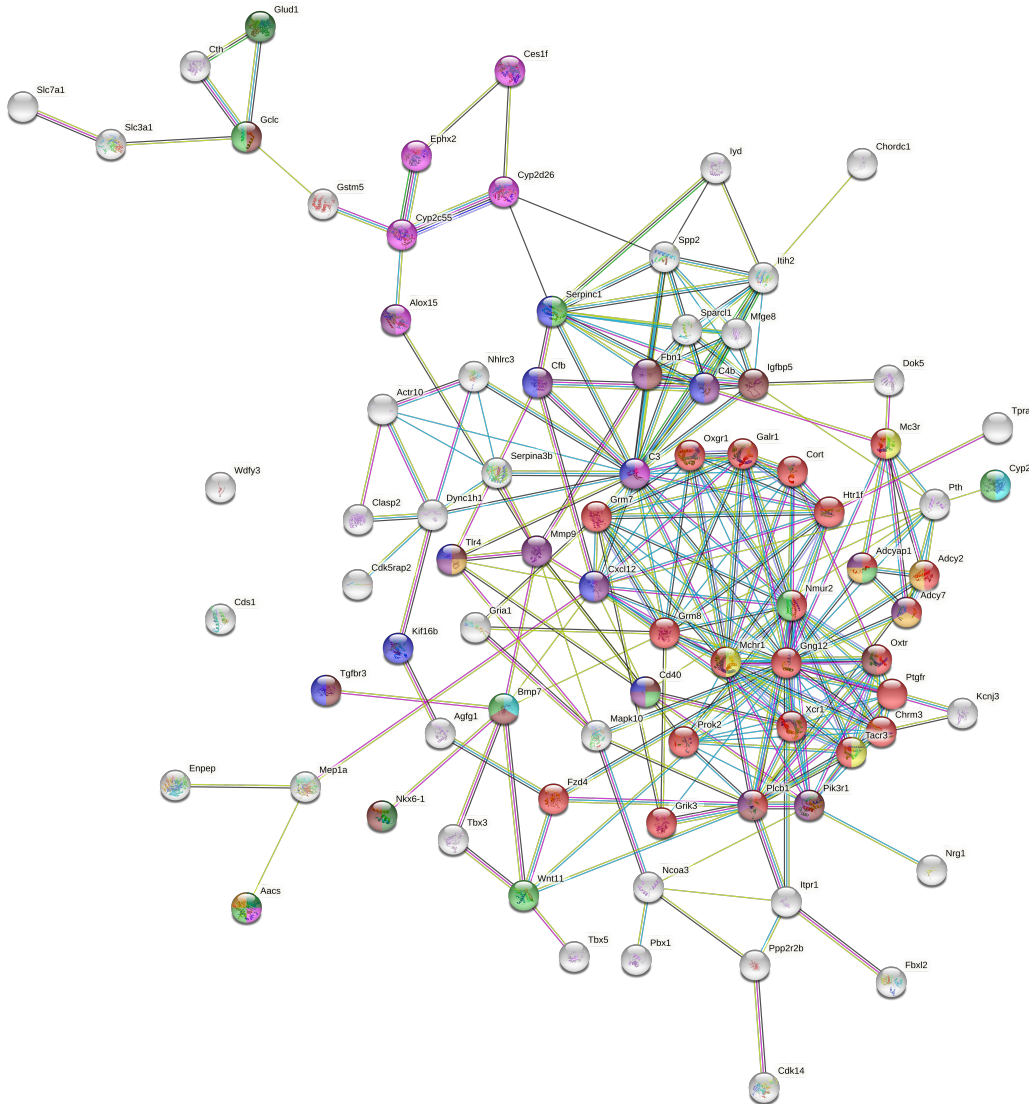
324 To further validate our results, we compared the list of genes contained within
325 intervals of our study to a list of differentially expressed protein between germ-free and
326 conventionally raised mice (Mills et al., 2020). This comparison was made based on the
327 general expectation that genes associated with variation in microbial abundances would
328 be more likely to differ according to the colonization status of the host. Thus, we
329 examined the intersection between genes identified in our study and the proteins
330 identified as highly associated ($|\pi| > 1$) with the colonization state of the colon and the
331 small intestine (Mills et al., 2020). Out of the 373 over- or under-expressed proteins
332 according to colonization status, we find 198 of their coding genes to be among our
333 significant loci, of which 17 are the closest genes to a significant marker (*Iyd*, *Nln*,
334 *Slc26a3*, *Slc3a1*, *Myom2*, *Nebl*, *Tent5a*, *Fxr1*, *Cbr3*, *Chrodc1*, *Nucb2*, *Arhgef10l*, *Sucla2*, *Enpep*,
335 *Prkca*, *Aacs*, and *Cox7c*). This is significantly more than expected by chance (simulated
336 $P = .0156$, 10 000 permutations). Further, analyzing the protein-protein interactions with
337 STRING results in a significant network ($P = 1.73 \times 10^{-14}$, and average node degree 2.4,

338 Suppl. Fig. 11), with *Cyp2c65*, *Cyp2c55*, *Cyp2b10*, *Gpx2*, *Cth*, *Eif3k*, *Eif1*, *Sucla2*, and *Rpl17*
339 identified as hub genes (Suppl. Fig. 12).

340 Subsequently, we merged the information from Mills et al. (2020) and the seven
341 previous QTL mapping studies discussed above to further narrow down the most
342 promising candidate genes, and found 30 genes overlapping with our study. Of these 30
343 genes, six are the closest gene to a significant SNP. These genes are myomesine 2
344 (*Myom2*), solute carrier family 3 member 1 (*Slc3a1*), solute carrier family 26 member 3
345 (*Slc26a3*), nebullette (*Neb1*), carbonyl reductase 3 (*Cbr3*), and acetoacetyl-coA synthetase
346 (*Aacs*).

347 *Candidate genes influencing bacterial abundance*

348 Finally, all previously mentioned candidate genes were combined in one gene set of
349 304 genes and compiled in a highly significant PPI network ($P < 1.0 \times 10^{-16}$, average node
350 degree=4.85, see Methods 4.13). Guided by this network, we filtered out genes situated
351 in the same genomic region and kept the gene with the highest connectivity and
352 supporting information (original network see Suppl. Fig. 13). This gave a resulting gene
353 set of 80 candidate genes (Fig. 6 and Suppl. Table 7). The G protein, GNG12 and the
354 complement component 3 C3, are the proteins with the most edges in the network (30
355 and 25, respectively), followed by MCHR1, CXCL12, and NMUR2 with each 18 edges.
356 Of these 80 highly connected genes, 66 are associated with bacteria that are either co-
357 speciating (co-speciation rate > 0.5 ; Groussin et al., 2017) and/or have high heritability
358 (> 0.5) suggesting a functionally important role for these bacterial taxa (Suppl. Table 7).



359 **Figure 6:** Network of host candidate genes influencing bacterial traits using
360 STRING (<https://string-db.org>). The nodes represent proteins and are colored ac-
361 cording to a selection of enriched GO terms and pathways: G protein coupled re-
362 ceptor (GPCR) signaling (red), regulation of the immune system process (blue), re-
363 sponse to nutrient levels (light green), fatty acid metabolic process (pink), glucose
364 homeostasis (purple), response to antibiotic (orange), regulation of feeding behavior
365 (yellow), positive regulation of insulin secretion (dark green), circadian entrainment
366 (brown), and response to vitamin D (turquoise). The color of the edges represents
367 the interaction type: known interactions from curated databases (turquoise) or ex-
368 perimentally determined (pink); predicted interactions from gene neighborhood
369 (green), gene fusions (red), gene co-occurrence (blue); other interactions from text-
370 mining (light green), co-expression (black), and protein homology (purple).

371 Discussion

372 Understanding the forces that shape variation in host-associated bacterial
373 communities within host species is key to understanding the evolution and maintenance
374 of meta-organisms. Although numerous studies in mice and humans demonstrate that
375 host genetics influences gut microbiota composition (McKnite et al., 2012; Leamy et al.,
376 2014; Goodrich et al., 2014; Org et al., 2015; Davenport et al., 2015; Wang et al., 2016;
377 Bonder et al., 2016; Goodrich et al., 2016; Kemis et al., 2019; Suzuki et al., 2019; Ishida et
378 al., 2020; Hughes et al., 2020; Rühlemann et al., 2021), our study is unique in a number of
379 important ways. First, the unique genetic resource of mice collected from a naturally
380 occurring hybrid zone together with their native microbes yielded extremely high
381 mapping resolution and the possibility to uncover ongoing evolutionary processes in
382 nature. Second, our study is the first to perform genetic mapping of 16S rRNA
383 transcripts in the gut environment, which was previously shown to be superior to DNA-
384 based profiling in a genetic mapping study of the skin microbiota (Belheouane et al.,
385 2017). Third, our study is one of the only to specifically examine the mucosa-associated
386 community. It was previously reasoned that the mucosal environment may better reflect
387 host genetic variation (Spor et al., 2011), and evidence for this hypothesis exists in nature
388 (Linnenbrink et al., 2013). Finally, by cross-referencing our results with previous
389 mapping studies and recently available proteomic data from germ-free versus
390 conventional mice, we curated a more reliable list of candidate genes and pathways.
391 Taken together, these results provide unique and unprecedented insight into the genetic
392 basis for host-microbe interactions.

393 Importantly, by using wild-derived hybrid inbred strains to generate our mapping
394 population, we gained insight into the evolutionary association between hosts and their
395 microbiota at the transition from within species variation to between species divergence.
396 Genetic relatedness in our mapping population significantly correlates with microbiome
397 similarity, supporting a basis for codiversification at the early stages of speciation. A
398 substantial proportion of microbial taxa are heritable, and heritability is correlated with
399 cospeciation rates. This suggests that (i) vertical transmission could enable greater host
400 adaptation to bacteria and/or (ii) the greater number of host genes associated with
401 cospeciating taxa could indicate a greater dependency on the host, such that survival
402 outside a specific host is reduced, making horizontal transmission less likely.

403 By performing 16S rRNA gene profiling at both the DNA and RNA level, we found
404 that 30% (DNA-based) to 45% (RNA-based) of bacterial taxa are heritable, which is
405 consistent with or higher than estimates reported in humans (~10%, Goodrich et al.,
406 2016; ~21%, Turpin et al., 2016) and previous mouse studies (Kovacs et al., 2011; McKnite
407 et al., 2012; Campbell et al., 2012; O'Connor et al., 2014; Carmody et al., 2015; Korach-
408 Rechtman et al., 2019;). The high proportion of heritable taxa, with estimates of up to
409 91%, is likely explained in part by several factors of our study design. First, mice were

410 raised in a controlled common environment, and heritability estimates in other
411 mammals were shown to be contingent on the environment (Grieneisen et al., 2021).
412 Further, bacterial communities were sampled from cecal tissue instead of fecal content
413 (Linnenbrink et al., 2013), and genetic variation was higher than in a typical mapping
414 study due to subspecies differences. For the RNA-based traits, heritability estimates
415 were significantly correlated with previously reported cospeciation rates in mammals
416 (Groussin et al., 2017). This pattern, as well as the higher proportion of heritable taxa in
417 RNA-based traits, suggest that host genetic effects are more strongly reflected by
418 bacterial activity than cell number.

419 Accordingly, we found a total of 179 and 313 unique significant loci for DNA-based
420 and RNA-based bacterial abundance, respectively, passing the conservative study-wide
421 significance threshold. Taxa had a median of five significant loci, suggesting a complex
422 and polygenic genetic architecture affecting bacterial abundances. We identify a higher
423 number of loci in comparison to previous QTL and GWAS studies in mice (Benson et al.,
424 2010; McKnite et al., 2012; Leamy et al., 2014; Wang et al., 2015; Org et al., 2015; Snijders
425 et al., 2016; Kemis et al., 2019), which may be due to a number of factors. The parental
426 strains of our study were never subjected to rederivation and subsequent reconstitution
427 of their microbiota, and natural mouse gut microbiota are more variable than the
428 artificial microbiota of laboratory strains (Kohl and Dearing, 2014; Weldon et al., 2015;
429 Suzuki, 2017; Rosshart et al., 2017;). Furthermore, as noted above, our mapping
430 population harbors both within- and between-subspecies genetic variation. We crossed
431 incipient species sharing a common ancestor ~ 0.5 million years ago, hence we may also
432 capture the effects of mutations that fixed rapidly between subspecies due to strong
433 selection, which are typically not variable within species (Walsh, 1998; Barton and
434 Keightley, 2002).

435 Importantly, our results also help to describe general features of the genetic
436 architecture of bacterial taxon activity. For the majority of loci, the allele associated with
437 lower relative abundance of the bacterial taxon was (partially) dominant. This suggests
438 there is strong purifying selection against a high abundance of any particular taxon,
439 which may help ensure high alpha diversity. The heterozygotes of one-third of
440 significant SNPs displayed transgressive phenotypes. This is consistent with previous
441 studies of hybrids (Turner et al., 2012; Turner and Harr, 2014; Wang et al., 2015;), for
442 example, wild-caught hybrids showed broadly transgressive gut microbiome
443 phenotypes. This pattern can be explained by over- or underdominance, or by epistasis
444 (Rieseberg et al., 1999).

445 Notably, many loci significantly associated with bacterial abundance in this study
446 were implicated in previous studies (Fig. 5). For example, chromosome 2 169-171 Mb is
447 associated with ASV23 (*Eisenbergiella*), *Eisenbergiella* and ASV32 (unclassified
448 Lachnospiraceae) in this study, and overlaps with significant loci from three previous
449 studies (Leamy et al., 2014; Snijders et al., 2016; Kemis et al., 2019). This region contains

450 eight protein-coding genes: *Gm11011*, *Znf217*, *Tshz2*, *Bcas1*, *Cyp24a1*, *Pfdn4*,
451 *4930470P17Rik*, and *Dok5*. Another hotspot is on chromosome 5 101-103 Mb. This locus is
452 significantly associated with four taxa in this study (Prevotellaceae, *Paraprevotella*, ASV7
453 genus *Paraprevotella* and *Acetatifactor*) and overlaps with associations for Clostridiales,
454 Clostridiaceae, Lachnospiraceae, and Deferribacteriaceae (Snijders et al., 2016). Protein-
455 coding genes in this region are: *Nkx6-1*, *Cds1*, *Wdfy3*, *Arhgap24*, and *Mapk10*. As previous
456 studies were based on rederived mouse strains, identifying significant overlap in the
457 identification of host loci suggests that some of the same genes and/or mechanisms
458 influencing major members of gut microbial communities are conserved even in the face
459 of community 'reset' in the context of re-derivation. The identity of the taxa is however
460 not always the same, which suggests that functional redundancy may contribute to
461 these observations, if e.g. several bacterial taxa fulfill the same function within the gut
462 microbiome (Moya and Ferrer, 2016; Tian et al., 2020). Additionally, there is significant
463 overlap of genes within loci identified in the current study and proteins differentially
464 expressed in the intestine of germ-free mice compared to conventionally raised mice
465 (Mills et al., 2020). Finally, by analyzing the functions of the genes closest to significant
466 SNPs, we found that 12 of the 14 significantly enriched KEGG pathways were shown to
467 be related to interactions with bacteria (Fonken et al., 2010; Thaïss et al., 2014; Neumann
468 et al., 2014; Thaïss et al., 2015a; Thaïss et al., 2015b; Castoldi et al., 2015; Erdman and
469 Poutahidis, 2016; Thaïss et al., 2016; Deaver et al., 2018; Wu et al., 2018; Peng et al., 2020;
470 Nagpal et al., 2020; Hollander and Kaunitz, 2020; Suppl. Table 5).

471 To improve the robustness of our results, we combined multiple lines of evidence to
472 prioritize candidates, resulting in a network of 80 genes (Suppl. Table 7). At the center of
473 this network is a set of 22 proteins involved in G-protein coupled receptor signaling (Fig.
474 6, red nodes). MCHR1, NMUR2, and TACR3 (Fig. 6, yellow) are known to regulate
475 feeding behavior (Saito et al., 1999; Cardoso et al., 2012; Smith et al., 2019), and CHRM3
476 to control digestion (Gautam et al., 2006; Tanahashi et al., 2009). Gut microbes can
477 produce GPCR agonists to elicit host cellular responses (Cohen et al., 2017; Colosimo et
478 al., 2019; Chen et al., 2019; Pandey et al., 2019). Thus, GPCRs may be key modulators of
479 communication between the gut microbiota and host. Another interesting group of
480 genes are those responding to nutrient levels (*Bmp7*, *Cd40*, *Aacs*, *Gclc*, *Nmur2*, *Cyp24a1*,
481 *Adcyap1*, *Serpinc1*, and *Wnt11*) (Sethi and Vidal-Puig, 2008; Peier et al., 2009; Townsend et
482 al., 2012; Yi and Bishop, 2015; Shi and Tu, 2015; Toderici et al., 2016; Yasuda et al., 2021;
483 Gastelum et al., 2021;), as gut microbiota affect host nutrient uptake (Chung et al., 2018).
484 In addition, CYP24A1, BMP7 and CD40 respond to vitamin D. Previous studies
485 identified vitamin D/the vitamin D receptor to play a role in modulating the gut
486 microbiota (Wang et al., 2016; Malaguarnera, 2020; Yang et al., 2020b; Singh et al., 2020),
487 and CD40 is known to induce a vitamin D dependent antimicrobial response through
488 IFN- γ activation (Klug-Micu et al., 2013).

489 Another important category of candidate genes are those involved in immunity.
490 Our most significant SNP was situated downstream of the *Tlr4* gene and was associated
491 with the genus *Dorea* and several *Dorea* species. *Dorea* is a known short chain fatty acid
492 producer (Taras et al., 2002; Reichardt et al., 2018) and interacts with tight junction
493 proteins *Claudin-2* and *Occludin* (Alhasson et al., 2017). *Tlr4* is a member of the Toll-like
494 receptor family, and has been linked with obesity, inflammation, and changes in the gut
495 microbiota (Velloso et al., 2015). These combined results reflect an important role for
496 *Dorea* in fatty acid harvesting and intestinal barrier integrity, both of which could act
497 systemically to activate TLR4 and to promote metabolic inflammation (Cani et al., 2008;
498 Delzenne et al., 2011; Nicholson et al., 2012). Moreover, the SNP with the second lowest
499 *P* value was associated with the same taxa and situated 181 kb upstream of *Irak4*. IRAK4
500 is rapidly recruited after TLR4 activation to enable downstream activation of the NFκB
501 immune pathway. *Irak4* has previously been associated with a change in bacterial
502 abundance using inbred mice (McKnite et al., 2012; Org et al., 2015).

503 Finally, we identified notable links between candidate genes and five human
504 diseases (mental disorders, blood pressure finding, systemic arterial pressure, substance-
505 related disorders, and atrial septal deficits; Suppl. Fig. 10). The connection to mental
506 disorders is intriguing as involvement of the gut microbiota is suspected (Kelly et al.,
507 2015; Foster et al., 2017; Cox and Weiner, 2018; Chen et al., 2019; Sarkar et al., 2020;
508 Parker et al., 2020; Flux and Lowry, 2020). Taken together with our finding of an
509 enriched set of GPCRs, this highlights the importance of host-microbial interplay along
510 the gut-brain axis. Moreover, we also identify a significant over-representation of IBD
511 genes (Khan et al., 2021) among the 925 genes nearest to significant SNPs (Suppl. Table
512 6). Interestingly, SNPs in five out of 14 genes are associated with ASVs belonging to the
513 genus *Oscillibacter*, a highly cospeciating taxon known to decrease during the active state
514 of IBD (Metwaly et al., 2020).

515 In summary, our study provides a number of novel insights into the importance of
516 host genetic variation in shaping the gut microbiome, in particular for cospeciating
517 bacterial taxa. These findings provide an exciting foundation for future studies of the
518 precise mechanisms underlying host-gut microbiota interactions in the mammalian gut
519 and should encourage future genetic mapping studies that extend analyses to the
520 functional metagenomic sequence level.

521 Materials and Methods

522 *Intercross design*

523 We generated a mapping population using partially inbred strains derived from
524 mice captured in the *M. m. musculus* - *M. m. domesticus* hybrid zone around Freising,
525 Germany in 2008 (Turner et al., 2012). Originally, four breeding stocks were derived
526 from 8-9 ancestors captured from one (FS, HA, TU) or two sampling sites (HO), and
527 maintained with four breeding pairs per generation using the HAN-rotation out-
528 breeding scheme (Rapp, 1972). Eight inbred lines (two per breeding stock) were
529 generated by brother/sister mating of the 8th generation lab-bred mice. We set up the
530 cross when lines were at the 5th-9th generation of brother-sister meeting, with
531 inbreeding coefficients of > 82%.

532 We first set up eight G1 crosses, each with one predominantly *domesticus* line (FS,
533 HO - hybrid index <50%; see below) and one predominantly *musculus* line (HA, TU -
534 hybrid index >50%); each line was represented as a dam in one cross and sire in another
535 (Suppl. Fig. 14). One line, FS5, had a higher hybrid index than expected, suggesting
536 there was a misidentification during breeding (see genotyping below). Next, we set up
537 G2 crosses in eight combinations (subcrosses), such that each G2 individual has one
538 grandparent from each of the initial four breeding stocks. We included 40 males from
539 each subcross in the mapping population.

540 This study was performed according to approved animal protocols and in-
541 stitutional guidelines of the Max Planck Institute. Mice were maintained and handled in
542 accordance with FELASA guidelines and German animal welfare law (Tierschutzgesetz
543 § 11, permit from Veterinäramt Kreis Plön: 1401-144/PLÖ-004697).

544 *Sample collection*

545 Mice were sacrificed at 91 ± 5 days by CO₂ asphyxiation. We recorded body weight,
546 body length and tail length, and collected ear tissue for genotyping. The caecum was
547 removed and gently separated from its contents through bisection and immersion in
548 RNAlater (Thermo Fisher Scientific, Schwerte, Germany). After overnight storage in
549 RNAlater at 4° C, the RNAlater was removed and tissue stored at -20° C.

550 *DNA extraction and sequencing*

551 We simultaneously extracted DNA and RNA from caecum tissue samples using
552 Qiagen (Hilden, Germany) Allprep DNA/RNA 96-well kits. We followed the
553 manufacturer's protocol, with the addition of an initial bead beating step using Lysing
554 matrix E tubes (MP Biomedical, Eschwege) to increase cell lysis. We used caecum tissue
555 because host genetics has a greater influence on the microbiota at this mucosal site than
556 on the lumen contents (Linnenbrink et al., 2013). We performed reverse transcription of
557 RNA with High-Capacity cDNA Transcription Kits from Applied Biosystems
558 (Darmstadt, Germany). We amplified the V1-V2 hypervariable region of the 16S rRNA

559 gene using barcoded primers (27F-338R) with fused MiSeq adapters and heterogeneity
560 spacers following (Rausch et al., 2016) and sequenced amplicons with 250 bp paired-
561 reads on the Illumina MiSeq platform.

562 *16S rRNA gene analysis*

563 We assigned sequences to samples by exact matches of MID (multiplex identifier, 10
564 nt) sequences processed 16S rRNA sequences using the DADA2 pipeline, implemented
565 in the DADA2 R package, version 1.16.0 (Callahan et al., 2016; Callahan, 2016). Briefly,
566 raw sequences were trimmed and quality filtered with the maximum two 'expected
567 errors' allowed in a read, paired sequences were merged and chimeras removed. For all
568 downstream analyses, we rarefied samples to 10,000 reads each. Due to the quality
569 filtering, we have phenotyping data for 286 individuals on DNA level, and 320 G2
570 individuals on RNA level. We classified taxonomy using the Ribosomal Database Project
571 (RDP) training set 16 (Cole et al., 2014). Classifications with low confidence at the genus
572 level (<0.8) were grouped in the arbitrary taxon 'unclassified_group'.

573 We used the phyloseq R package (version 1.32.0) to estimate alpha diversity using
574 the Shannon index and Chao1 index, and beta diversity using Bray-Curtis distance
575 (McMurdie and Holmes, 2013). We defined core microbiomes at the DNA- and RNA-
576 level, including taxa present in > 25% of the samples and with median abundance of
577 non-zero values > 0.2% for amplicon sequence variant (ASV) and genus; and >0.5% for
578 family, order, class and phylum.

579 *Genotyping*

580 We extracted genomic DNA from ear samples using Qiagen Blood and Tissue 96
581 well kits (Hilden, Germany), according to the manufacturer's protocol. We sent DNA
582 samples from 26 G0 mice and 320 G2 mice to GeneSeek (Neogen, Lincoln, NE) for
583 genotyping using the Giga Mouse Universal Genotyping Array (GigaMUGA; Morgan et
584 al., 2015), an Illumina Infinium II array containing 141,090 single nucleotide
585 polymorphism (SNP) probes. We quality-filtered genotype data using plink 1.9 (Chang
586 et al., 2015); we removed individuals with call rates <90% and SNPs that were: not bi-
587 allelic, missing in >10% individuals, with minor allele frequency <5%, or Hardy-
588 Weinberg equilibrium exact test P values <1e-10. A total of 64,103 SNPs and all but one
589 G2 individual were retained. Prior to mapping, we LD-filtered SNPs with $r^2 > 0.9$ using a
590 window of 5 SNPs and a step size of 1 SNP. We retain 32,625 SNPs for mapping.

591 *Hybrid index calculation*

592 For each G0 and G2 mouse, we estimated a hybrid index – defined as the
593 percentage of *M. m. musculus* ancestry. We identified ancestry-informative SNP markers
594 by comparing GigaMUGA data from ten individuals each from two wild-derived
595 outbred stocks of *M. m. musculus* (Kazakhstan and Czech Republic) and two of *M. m.*
596 *domesticus* (Germany and France) maintained at the Max Planck Institute for

597 Evolutionary Biology (L.M. Turner and B. Payseur, unpublished data). We classified
598 SNPs as ancestry informative if they had a minimum of 10 calls per subspecies, the
599 major allele differed between *musculus* and *domesticus*, and the allele frequency
600 difference between subspecies was > 0.3 . A total of 48,361 quality-filtered SNPs from the
601 G0/G2 genotype data were informative, including 8,775 SNPs with fixed differences
602 between subspecies samples.

603 *Correlation between host relatedness and microbiome structure*

604 To investigate if host relatedness is correlated with individual variation in
605 microbiome composition, we computed a centered relatedness matrix using the 32,625
606 filtered SNPs with GEMMA (v 0.98.1; Zhou and Stephens, 2012) and microbial
607 composition-based kinship matrix among individuals based on relative bacterial
608 abundances (Chen et al., 2018). The kinship matrix was calculated with the formula:

$$Kinship = 1/p \sum_{i=1}^p (x_i - 1_n \bar{x}_i)(x_i - 1_n \bar{x}_i)^T$$

609 where X denotes the $n \times p$ matrix of genotypes or relative abundances, x_i as its i th
610 column representing the genotypes of i th SNP or the relative abundance of the i th ASV,
611 \bar{x}_i as the sample mean and 1_n as a $n \times 1$ vector of 1's. We used a Mantel test with the
612 Spearman's correlation to test for correlation between the host SNP-based kinship and
613 microbial composition-based kinship using 10,000 permutations.

614 *SNP-based heritability of microbial abundances*

615 We calculated SNP-based heritabilities for bacterial abundances using a linear
616 mixed model implemented in the lme4qtl R package (version 0.2.2; Ziyatdinov et al.,
617 2018). The SNP-based heritability is expressed as:

$$h^2 = \frac{\sigma_g^2}{\sigma_g^2 + \sigma_m^2 + \sigma_e^2}$$

618 where σ_g^2 is the genetic variance estimated by K_{SNP} , σ_m^2 variance of the mating pair
619 component, and σ_e^2 the variance due to residual environmental factors. We determined
620 significance of the heritability estimates using exact likelihood ratio tests, following
621 Supplementary Note 3 in Ziyatdinov et al., 2018, using the exactLRT() function of the R
622 package RLRsim (version 3.1-6; Fabian et al., 2008).

623 *Genome-wide association mapping*

624 Prior to mapping, we inverse logistic transformed bacterial abundances using the
625 inv.logit function from the R package gtools (version 3.9.2; Gregory R. Warnes, 2020).

626 We performed association mapping in the R package lme4qtl (version 0.2.2;
627 Ziyatdinov et al., 2018) with the following linear mixed model:

$$y_i = \mu + a_i X_{ij}^a + d_i X_{ij}^d + Wu + e$$

628

629 where y_j is the phenotypic value of the j th individual; μ is the mean, X_{ij} the additive
630 and X_{ij}^d the dominance genotypic index values coded as for individual j at locus i . a and
631 d indicate fixed additive and dominance effects, W indicates random effects mating pair
632 and kinship matrix, plus residual error e .

633 We estimated additive and dominance effects separately because we expected to
634 observe underdominance and overdominance in our hybrid mapping population, as
635 well as additive effects, and aimed to estimate their relative importance. To model the
636 additive effect (i.e. 1/2 distance between homozygous means), genotypes at each locus,
637 i , were assigned additive index values ($X^a \in 1, 0, -1$) for AA, AB, BB, respectively, with A
638 indicating the major allele and B the minor allele. To model dominance effects (i.e.
639 heterozygote mean - midpoint of homozygote means), genotypes were assigned
640 dominance index values ($X^d \in 0, 1$) for homozygotes and heterozygotes, respectively.

641 We included mating pair as a random effect to account for maternal effects and cage
642 effects, as male litter mates are kept together in a cage after weaning. We included
643 kinship coefficient as a random effect in the model to account for population and family
644 structure. To avoid proximal contamination, we used a leave-one-chromosome-out
645 approach, that is, when testing each single-SNP association we used a relatedness matrix
646 omitting markers from the same chromosome (Parker et al., 2014). Hence, for testing
647 SNPs on each chromosome, we calculated a centered relatedness matrix using SNPs
648 from all other chromosomes with GEMMA (v0.97; Zhou and Stephens, 2012). We
649 calculated P values for single-SNP associations by comparing the full model to a null
650 model excluding fixed effects. Code for performing the mapping is available at [https://](https://github.com/sdoms/mapping_scripts)
651 github.com/sdoms/mapping_scripts.

652 We evaluated significance of SNP-trait associations using two thresholds; first, we
653 used a genome-wide threshold for each trait, where we corrected for multiple testing
654 across markers using the Bonferroni method (Abdi, 2007). Second, as bacteria interact
655 with each other within the gut as members of a community, bacterial abundances are
656 non-independent, so we calculated a study-wide threshold dividing the genome-wide
657 threshold by the number of effective taxa included. We used matSpDlite (Nyholt, 2019;
658 Li and Ji, 2005; Qin et al., 2020) to estimate the number of effective bacterial taxa based
659 on eigenvalue variance.

660 To estimate the genomic interval represented by each significant LD-filtered SNP,
661 we report significant regions defined by the most distant flanking SNPs in the full pre-
662 LD-filtered genotype dataset showing $r^2 > 0.9$ with each significant SNP. We combined
663 significant regions less than 10 Mb apart into a single region. Genes situated in

664 significant regions were retrieved using biomaRt (Steffen Durinck, 2009), and the mm10
665 mouse genome.

666 *Dominance analyses*

667 We classified dominance for SNPs with significant associations on the basis of the
668 d/a ratio (Falconer, 1996) where d is the dominance effect, a the additive effect. As the
669 expected value under purely additive effects is 0. As our mapping population is a multi-
670 parental-line cross, and not all SNPs were ancestry-informative with respect to *musculus/*
671 *domesticus*, the sign of a effects is defined by the major allele within our mapping
672 population, which lacks clear biological interpretation. To provide more meaningful
673 values, we report $d/|a|$, such that a value of 1 = complete dominance of the allele
674 associated with higher bacterial abundance, and a value of -1 = complete dominance of
675 the allele associated with lower bacterial abundance. Values above 1 or below -1 indicate
676 over/underdominance. We classified effects of significant regions the following
677 arbitrary $d/|a|$ ranges to classify dominance of significant regions (Burke et al., 2002;
678 Miller et al., 2014): underdominant <-1.25, high abundance allele recessive between -1.25
679 and -0.75, partially recessive between -0.75 and -0.25, additive between -0.25 and 0.25,
680 partially dominant between 0.25 and 0.75, dominant 0.75 and 1.25, and
681 overdominant >1.25.

682 *Gene ontology and network analysis*

683 The nearest genes up- and downstream of the significant SNPs were identified
684 using the locateVariants() function from the VariantAnnotation R package (version
685 1.34.0; Valerie et al., 2014) using the default parameters. A maximum of two genes per
686 locus were included (one upstream, and one downstream of a given SNP).

687 To investigate functions and interactions of candidate genes, we calculated a
688 protein-protein interaction (PPI) network with STRING version 11 (Szklarczyk et al.,
689 2019), on the basis of a list of the closest genes to all SNPs with significant trait
690 associations. We included network edges with an interaction score >0.9, based on
691 evidence from fusion, neighborhood, co-occurrence, experimental, text-mining,
692 database, and co-expression. We exported this network to Cytoscape v 3.8.2 (Shannon et
693 al., 2003) for identification of highly interconnected regions using the MCODE
694 Cytoscape plugin (Bader and Hogue, 2003), and functional annotation of clusters using
695 the stringApp Cytoscape plugin (Doncheva et al., 2019).

696 We identified overrepresented KEGG pathways and human diseases using the
697 clusterProfiler R package (version 3.16.1; Yu et al., 2012). P values were corrected for
698 multiple testing using the Benjamini-Hochberg method. Pathways and diseases with an
699 adjusted P value < .05 were considered over-represented.

700 *Calculating overlap with other studies and over-representation of IBD genes*

701 To test for significant overlap with loci identified in previous mapping studies and
702 for over-representation of IBD genes, we used the tool *poverlap* (Brent Pedersen, 2013) to
703 compare observed overlap to random expectations based on 10,000 permutations of
704 significant regions. We identified genes within overlapping regions using the
705 `locateVariants()` function from the VariantAnnotation R package (version 1.34.0; Valerie
706 et al., 2014).

707 *Combination of results*

708 Hub genes SNP network and their first neighbors, the hub genes from the
709 'differentially expressed in GF mice'-network and their respective first neighbors, genes
710 found in both Mills et al. (2020) and other mouse QTL studies, closest genes to a SNP
711 found in Mills et al. (2020), genes situated in the 20 smallest intervals, six genes in the
712 two intervals with the lowest *P* values, twenty genes in intervals found in most different
713 taxa, genes situated in the region with most overlap within our study, and finally the
714 genes situated in the intervals that most frequently overlapped with other studies were
715 combined into one gene set and analyzed with STRING. Genes situated in the same
716 genomic locus were curated according to the number of edges in the STRING network.

717 **Data and code availability:** DNA- and RNA-based 16S rRNA gene sequences are
718 available under project accession number PRJNA759194. Code is available at [https://](https://github.com/sdoms/mapping_scripts)
719 [/github.com/sdoms/mapping_scripts](https://github.com/sdoms/mapping_scripts).

720 **Supplementary Materials:** Suppl. Fig 1-14, Suppl. Table 1: Heritability estimates,
721 Suppl. Table 2: Genome-wide significant associations, Suppl. Table 3: Study-wide
722 significant associations, Suppl. Table 4: Intervals smaller than 1Mb, Suppl. Table 5:
723 Over-represented KEGG pathways, Suppl. Table 6: IBD genes, Suppl. Table 7:
724 Candidate genes.

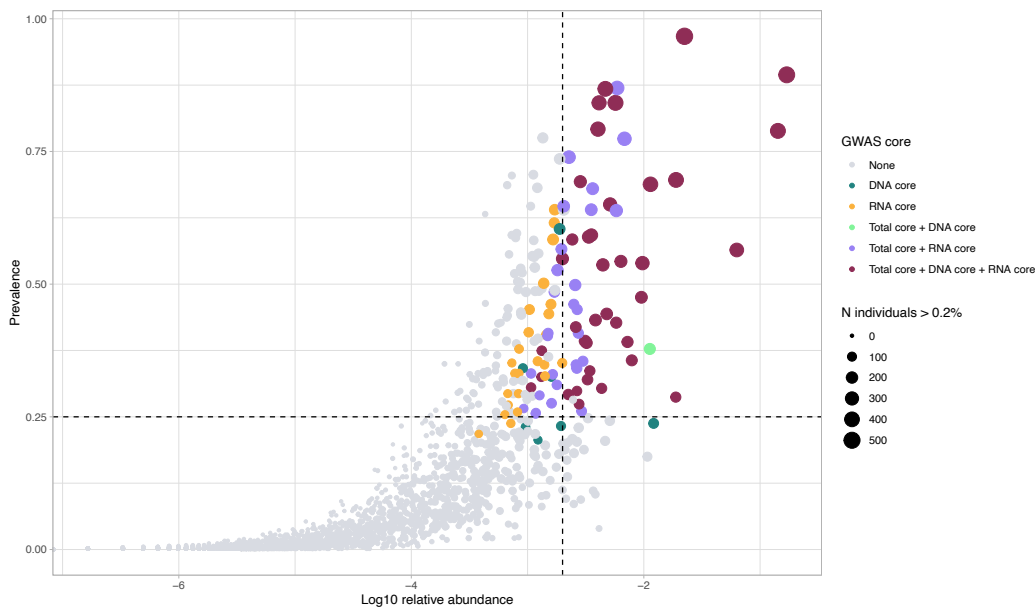
725 **Acknowledgments:** We thank Diethard Tautz for generous support of mouse
726 breeding and Camilo Medina and the MPI-Plön mouse team for performing mouse
727 husbandry, and Katja Cloppenburg-Schmidt and Dr. Sven Künzel for their excellent
728 technical assistance. We thank Mathieu Groussin for assistance with cospeciation rate
729 data. Research funding for this project was provided by the Deutsche
730 Forschungsgemeinschaft Collaborative Research Center 1182, 'Origin and Function of
731 Metaorganisms' (J.F.B. and A.F.) and TU 500/2-1 to L.M.T, and by the Max Planck
732 Society (to D. Tautz).

733 **Author contributions:** Conceptualization: L.M.T., S.I., A.F., and J.F.B; Methodology:
734 L.M.T, J.F.B., S.D., S.I., A.F., and A.K.; Software: S.D., M.R., and L.M.T; Validation: S.D.,
735 M.R., A.K., and L.M.T.; Formal Analysis: S.D., M.R., A.K., and L.M.T; Investigation: S.D.
736 and L.M.T.; Resources: S.D., H.F., and C.C; Writing - Original Draft: S.D.; Writing -

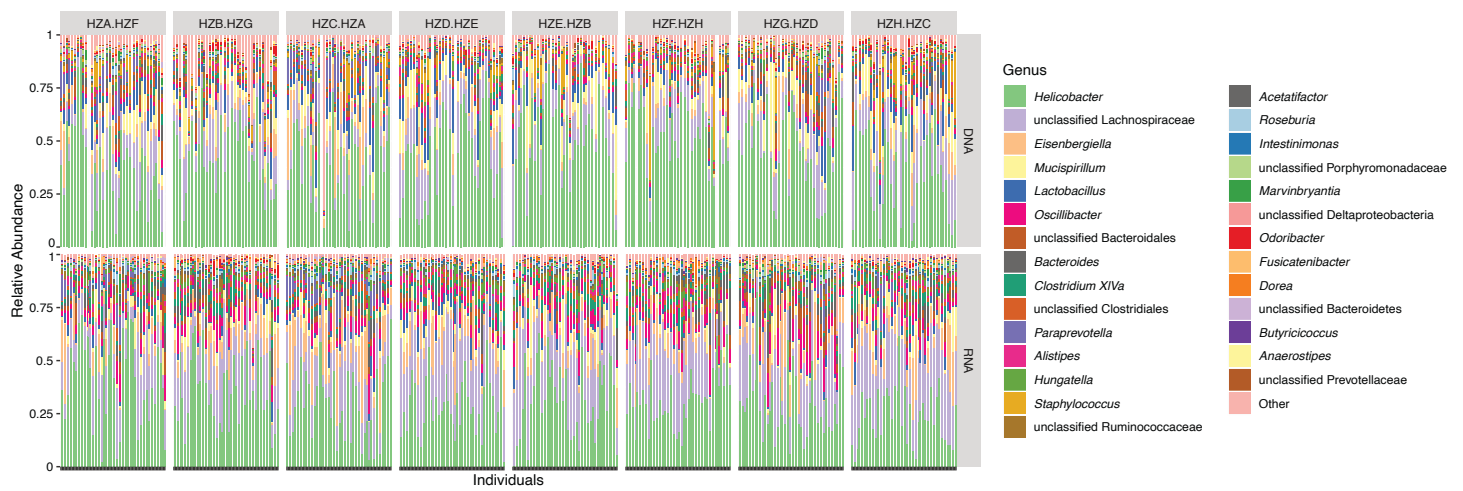
737 Review & Editing: S.D., L.M.T, and J.F.B; Visualization: S.D. and L.M.T; Supervision:
738 L.M.T, A.F, and J.F.B.; Project Administration: J.F.B.; Funding Acquisition: A.F, L.M.T,
739 and J.F.B.

740 **Conflicts of Interest: The authors declare no conflict of interest.**

741 Supplementary figures



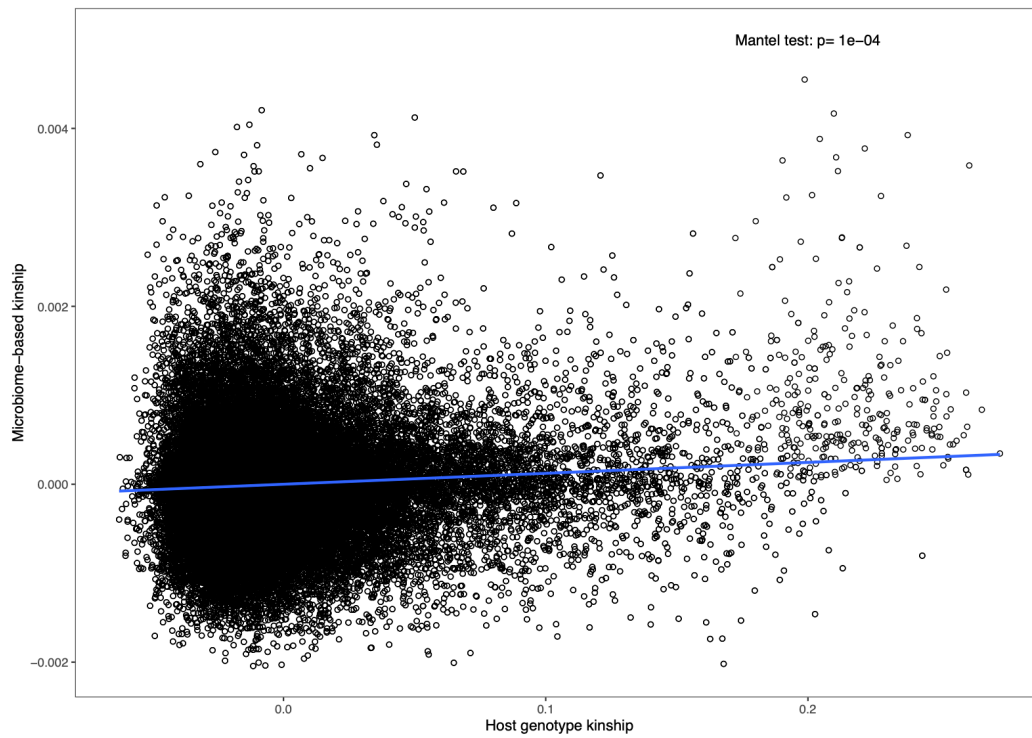
742 **Supplementary figure 1:** Selection of taxa for mGWAS analysis. A scatter plot showing the
743 association of average relative abundance of taxa with their prevalence in the G2 mapping
744 population. Taxa retained for analysis are colored according to the originating core. The size of
745 each dot represents the number of individuals that have a median abundance higher than 0.2% of
746 the taxon. The dashed lines represent the thresholds of the core (vertical: median abundance > 0.2%
747 and horizontal prevalence of 25 %).



748 **Supplementary figure 2: Relative abundances of core genera in G2 mapping population.**

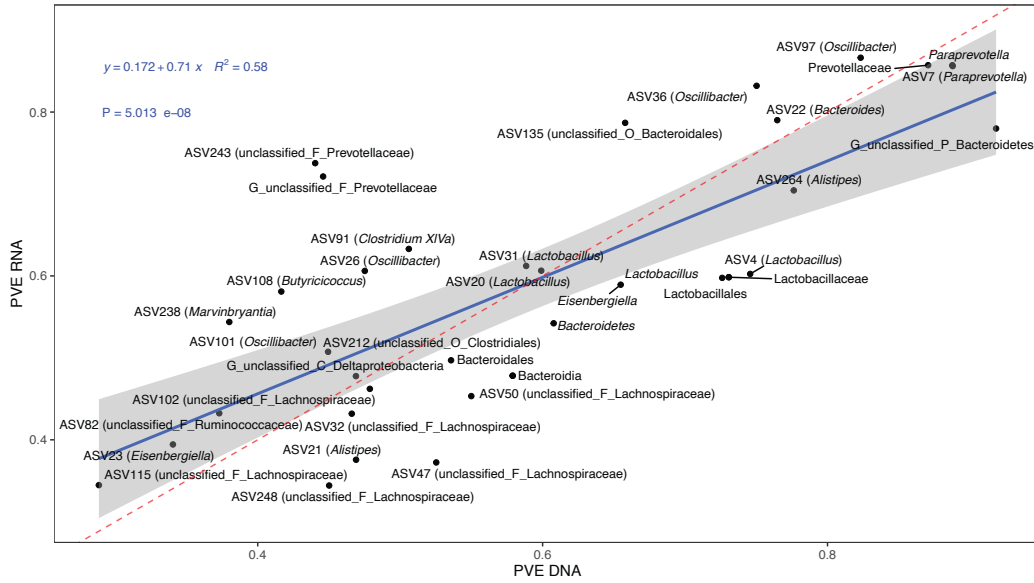
749 Each vertical line represents one individual. Subcross (see supplementary figure 14) is indicated at

750 the top.



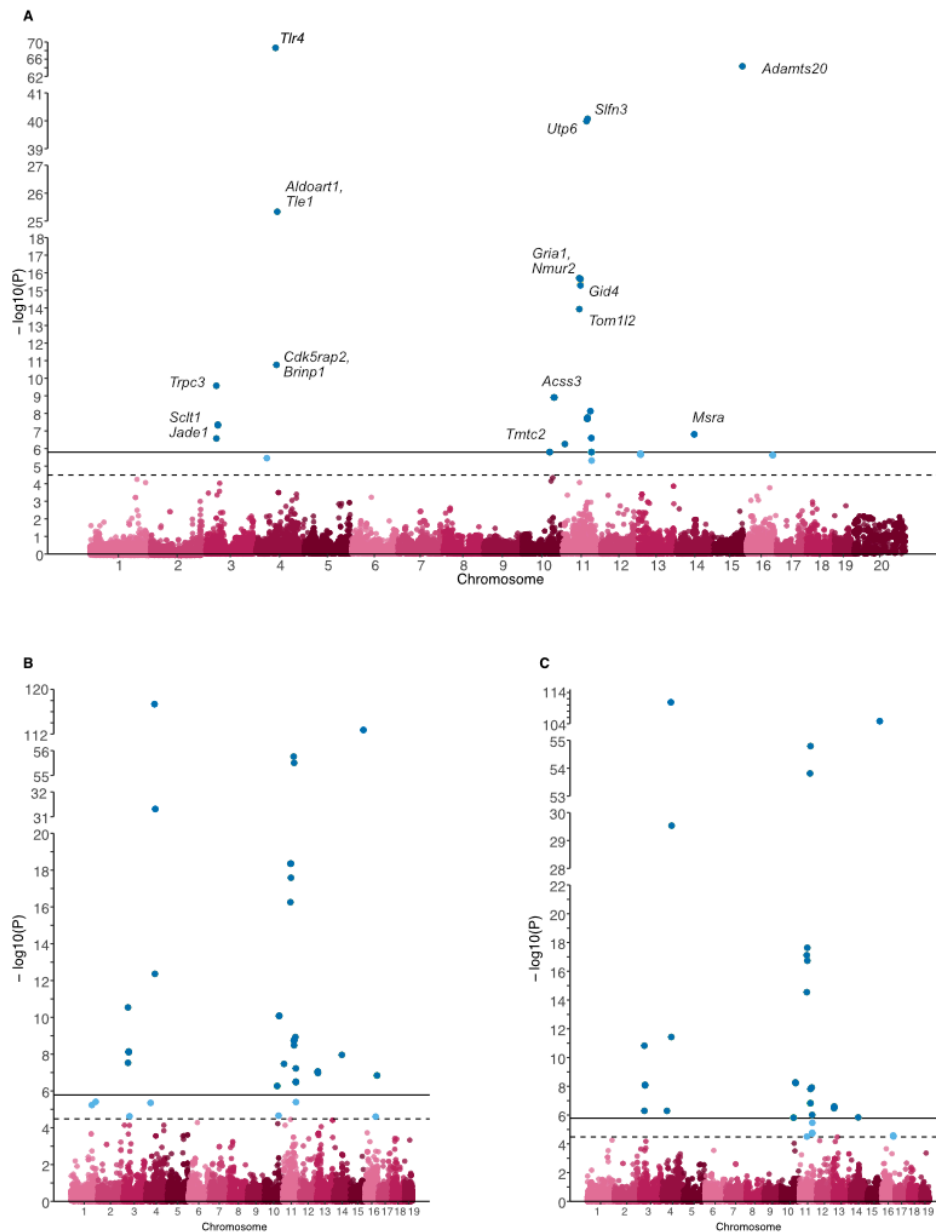
751
752
753

Supplementary figure 3: Host genetic relatedness calculated from SNP data (x-axis) correlated with microbial composition-based relatedness (y-axis) calculated from ASV abundances. The blue line represents a linear regression fit to the data.



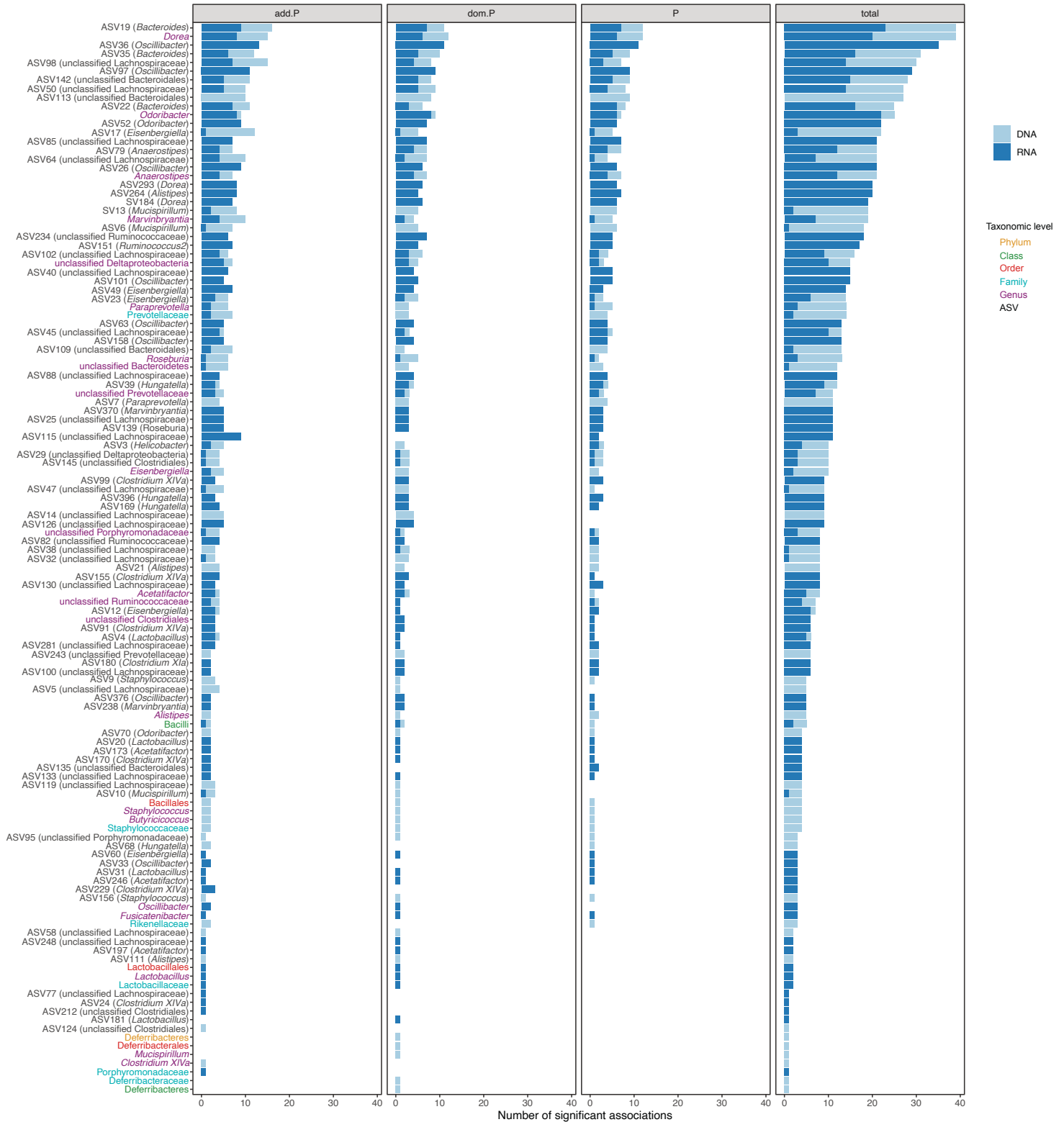
754
755
756

Supplementary figure 4: Correlation of SNP-based heritability estimates based on DNA (x-axis) or RNA (y-axis). The blue line represents a linear regression fit to the data. Red dashed line represents the identity line with a slope of 1.



757
758
759
760
761

Supplementary figure 5: Manhattan plots for ASV184 (*Dorea*) of the complete model (A), the additive effect (B) or the dominance effect (C). SNPs passing the study-wide significance threshold (solid line) are shown in dark blue, while genome-wide significant SNPs (dashed line) are shown in light blue. In panel A, the closest gene to the SNP is shown for a subset of significant SNPs.

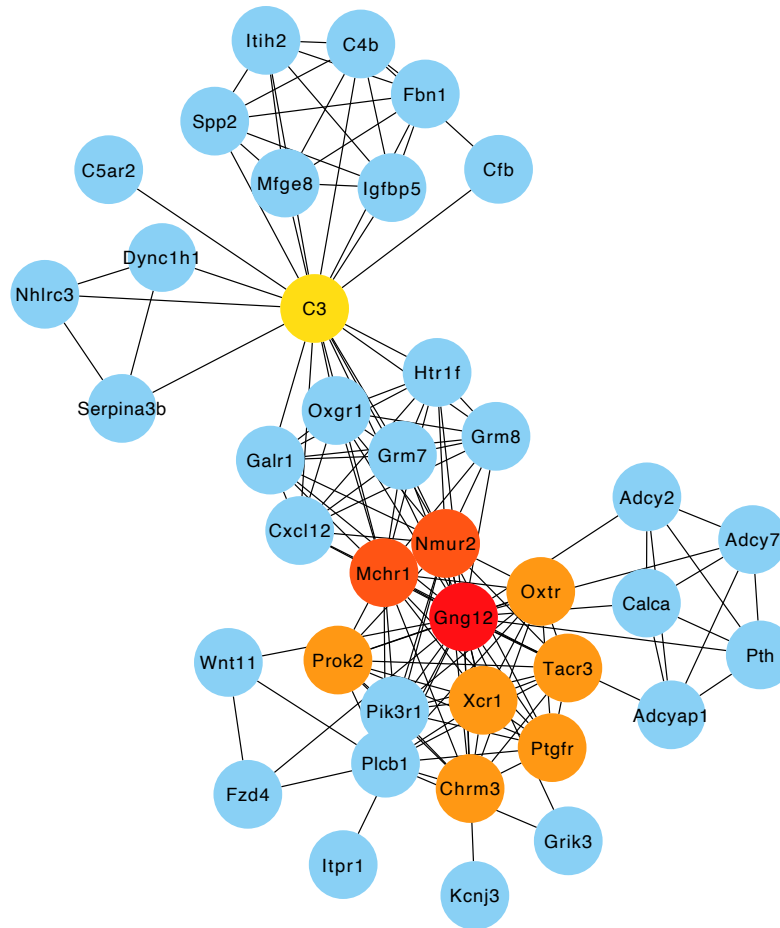


762

763

764

Supplementary figure 6: Number of significantly associated loci per bacterial taxon. Loci with significant additive effects (add.P), dominance effects (dom.P) or effects in full model (P) are indicated.



765

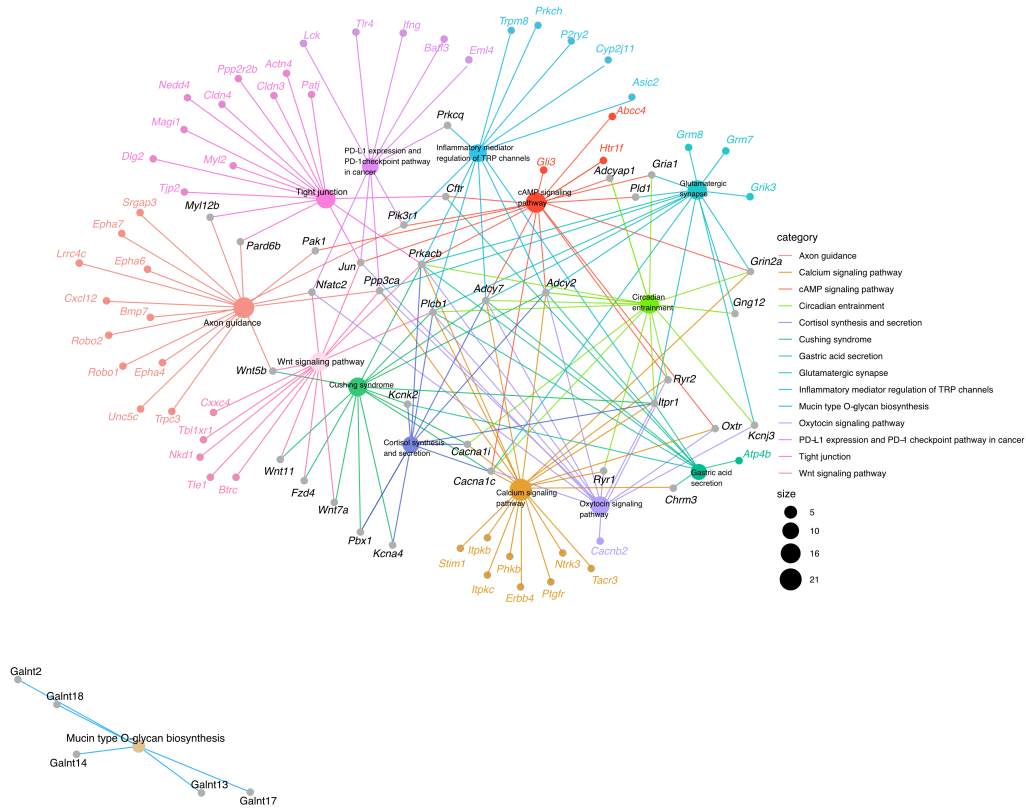
766

767

768

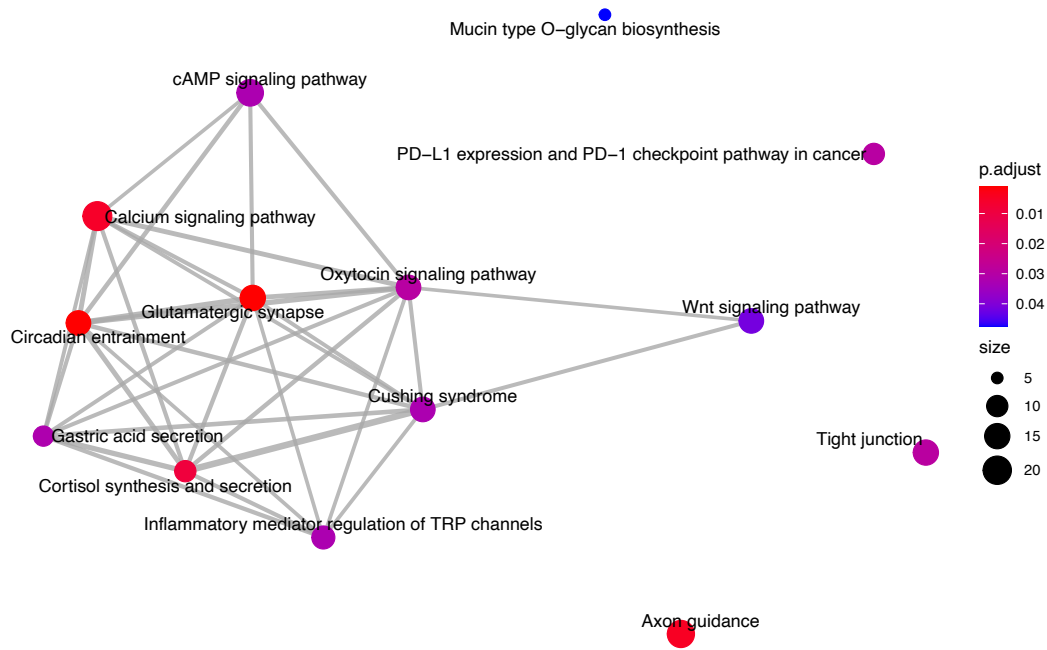
769

Supplementary figure 7: Top ten hub genes of the protein-protein interaction (PPI) network with the closest genes to the host SNPs significantly associated with bacterial abundances. The nodes are colored according to hub gene rank from 1 (red) to 10 (yellow). Blue nodes are the first neighbors.

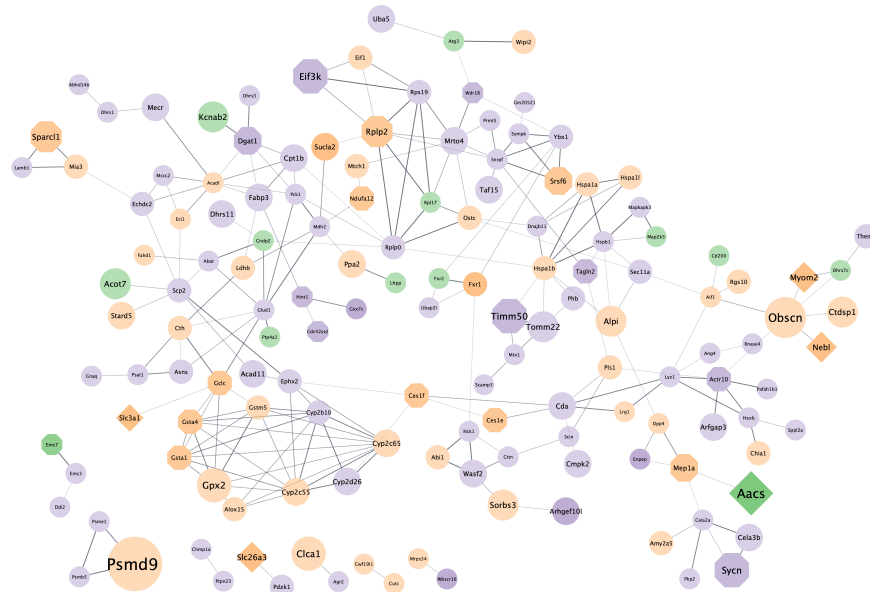


770
771

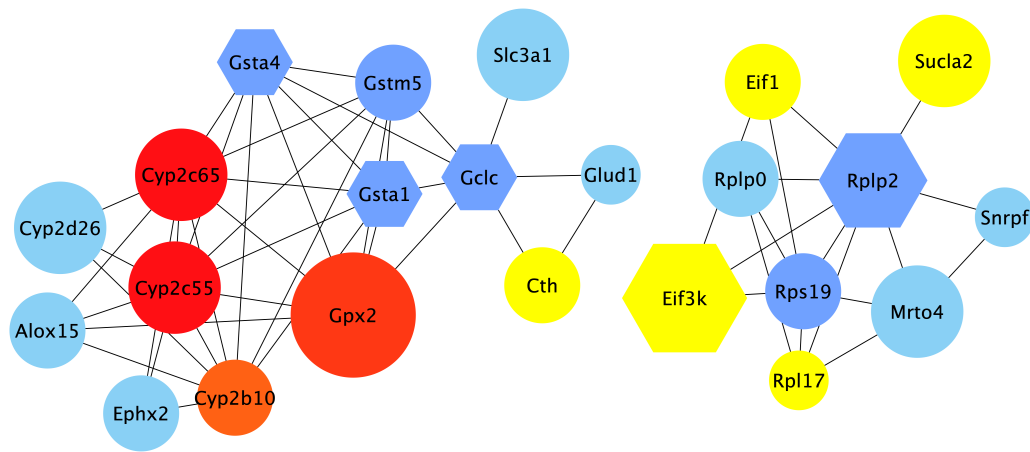
Supplementary figure 8: Genes belonging to over-represented KEGG pathways within the host genes closest to significant SNPs from association analysis.



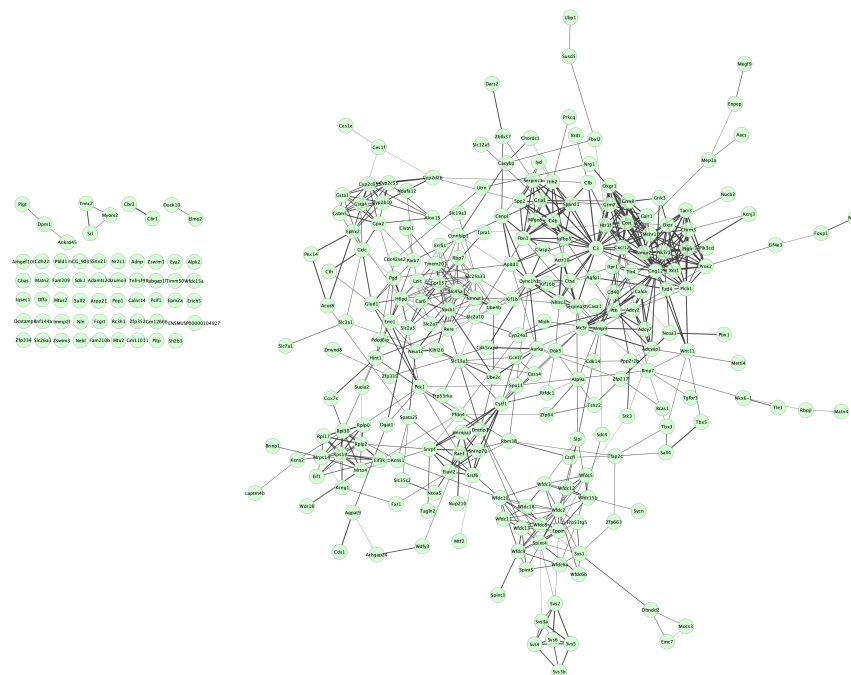
772 **Supplementary figure 9:** Enriched KEGG pathways among closest genes to significant SNPs from
773 association analysis. Node color indicates FDR-adjusted P value of enrichment and node size indi-
774 cates number of candidate genes in pathway.



777 **Supplementary figure 11:** STRING (Szklarczyk et al., 2019) protein-protein interaction network of
778 proteins that are differentially expressed in the intestine (small intestine and colon) of germ-free
779 (GF) mice compared to conventionally raised mice, found in the present study. The color of the
780 network nodes indicates whether the QTL hit was found using the DNA abundances (green),
781 RNA abundances (purple) or was found in both (orange). The shape represents if the gene of the
782 protein was the closest gene to the significant SNP (rectangle), if the gene was also found in QTLs
783 of other studies (octagon), a combination of both (diamond), or only differentially expressed in GF
784 mice vs. conventionally raised mice. The node size expresses the number of taxa where the gene
785 was found in a QTL. The edges represent protein-protein interactions, where the line thickness in-
786 dicates the strength of the data support from text mining, experiments, databases, co-expression,
787 gene-fusion, and co-occurrence.

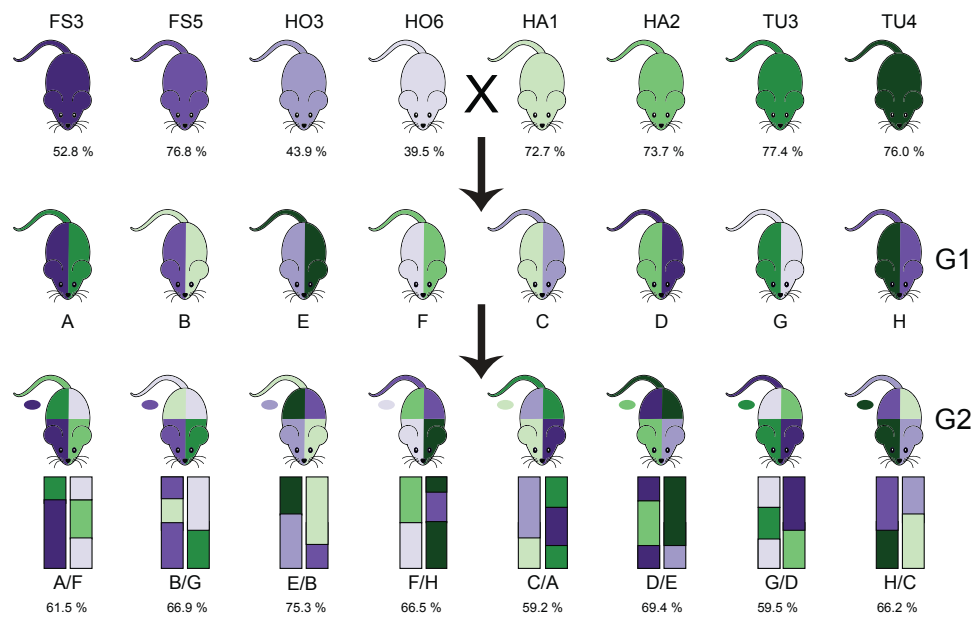


788 **Supplementary figure 12:** Visualization of the top hub genes calculated with the MCC algo-
789 rithm and their first neighbors from the protein-protein interaction (PPI) network of genes
790 found in intervals in present study that are also differentially expressed in germ-free versus
791 conventionally raised mice. Edges represent the protein-protein associations. The red nodes
792 represent genes with a high degree (= hub genes), and the yellow nodes with a low degree,
793 while the blue nodes represent their first neighbors. All nodes shown are differentially ex-
794 pressed in GF mice. Hexagon shaped nodes are genes/proteins also found associated with
795 gut microbiome abundances in other mouse QTL studies, and round nodes are 'only' differ-
796 entially expressed in GF mice. The size of the node is an indication of the amount of taxa as-
797 sociated with the gene.



798
799
800

Supplementary figure 13: Original protein protein interaction (PPI) network of 304 candidate genes closest to SNPs significantly associated with bacterial abundances. Generated in STRING (Szklarczyk et al., 2019) and Cytoscape (Shannon et al., 2003).



801 **Supplementary figure 14:** Overview of the intercross design. G0 mice are from eight partially
802 inbred lines derived from mice wild-caught in four hybrid zone sites. Hybrid index - the per-
803 centage of *musculus* alleles - is reported as the mean for the G0 mice from each line (top), or
804 mean of 40 G2s from each subcross (bottom). We performed eight G1 crosses with one line
805 with hybrid index ~50% (purple shades) and one line with hybrid index >50% (green
806 shades); color on the left side of mouse diagram indicates dam line and right side indicates
807 sire line. Next, G1 mice were crossed in eight combinations such that each G2 mouse had one
808 grandparent from each of the four breeding stocks, indicated by colors of mouse diagram,
809 and representative chromosomes below. Tail color indicates Y chromosome strain, and oval
810 indicates mitochondrial strain.

811 References

- 812** Abdi, Hervé (2007), ‘The Bonferonni and Šidák Corrections for Multiple Comparisons’, in Salkind, Neil J. (ed.), (Encyclopedia of Measurement and Statistics, SAGE), 9.
- 813**
- 814** Alhasson, Firas, et al. (2017), ‘Altered gut microbiome in a mouse model of Gulf War Illness causes neuroinflammation and intestinal injury via leaky gut and TLR4 activation’, *PLoS One*, 12 (3), e0172914.
- 815**
- 816** Amato, Katherine R, et al. (2019), ‘Evolutionary trends in host physiology outweigh dietary niche in structuring primate gut microbiomes’, *The ISME journal*, 13 (3), 576-87.
- 817**
- 818** Backhed, F., et al. (2004), ‘The gut microbiota as an environmental factor that regulates fat storage’, *Proceedings of the National Academy of Sciences*, 101 (44), 15718-23.
- 819**
- 820** Bader, Gary D. and Christopher WV Hogue (2003), ‘An automated method for finding molecular complexes in large protein interaction networks’, *BMC Bioinformatics*, 4 (1), 2.
- 821**
- 822** Barton, Nicholas H. and Peter D. Keightley (2002), ‘Understanding quantitative genetic variation’, *Nat. Rev. Genet.*, 3 (1), 11-21.
- 823**
- 824** Beavis, WD (1994), ‘The power and deceit of QTL experiments: lessons from comparative QTL studies’, Proceedings of the forty-ninth annual corn and sorghum industry research conference 250 266.
- 825**
- 826** Belheouane, Meriem, et al. (2017), ‘Improved detection of gene-microbe interactions in the mouse skin microbiota using high-resolution QTL mapping of 16S rRNA transcripts’, *Microbiome*, 5 (1), 1-17.
- 827**
- 828** Benson, Andrew K., et al. (2010), ‘Individuality in gut microbiota composition is a complex polygenic trait shaped by multiple environmental and host genetic factors’, *Proceedings of the National Academy of Sciences of the United States of America*
- 829**
- 830** *Proc. Natl. Acad. Sci. U.S.A.*, 107 (44), 18933-38.
- 831**
- 832** Bonder, Marc Jan, et al. (2016), ‘The effect of host genetics on the gut microbiome’, *Nat. Genet.*, 48 (11), 1407-12.
- 833** Brent Pedersen, Joe Brown (2013), ‘poverlap: significance testing over interval overlaps’,
- 834** Brooks, AW, et al. (2016), ‘Phylosymbiosis: Relationships and Functional Effects of Microbial Communities across Host Evolutionary History.’, *PLoS Biol.*, 14 (11), e2000225.
- 835**
- 836** Brucker, RM and SR Bordenstein (2012a), ‘Speciation by symbiosis.’, *Trends Ecol Evol*, 27 (8), 443-51.
- 837** Brucker, Robert M and Seth R Bordenstein (2012b), ‘The roles of host evolutionary relationships (genus: Nasonia) and development in structuring microbial communities’, *Evolution: International Journal of Organic Evolution*, 66 (2), 349-62.
- 838**
- 839**
- 840** Burke, John M., et al. (2002), ‘Genetic Analysis of Sunflower Domestication’, *Genetics*, 161 (3), 1257-67.
- 841** Callahan, Benjamin J (2016), ‘DADA2 pipeline’, *DADA2*,
- 842** Callahan, Benjamin J, et al. (2016), ‘DADA2: High resolution sample inference from Illumina amplicon data’, *Nature methods*
- 843**
- 844** *Nat Methods*, 13 (7), 581-83.
- 845** Campbell, JH, et al. (2012), ‘Host genetic and environmental effects on mouse intestinal microbiota.’, *ISME J*, 6 (11), 2033-44.
- 846**
- 847** Cani, Patrice D., et al. (2008), ‘Changes in gut microbiota control metabolic endotoxemia-induced inflammation in high-fat diet-induced obesity and diabetes in mice’, *Diabetes*, 57 (6), 1470-81.
- 848**
- 849** Carding, Simon, et al. (2015), ‘Dysbiosis of the gut microbiota in disease’, *Microb. Ecol. Health Dis.*, 26
- 850** Cardoso, JC, et al. (2012), ‘Feeding and the rhodopsin family g-protein coupled receptors in nematodes and arthropods.’, *Front Endocrinol (Lausanne)*, 3 157.
- 851**
- 852** Carmody, RN, et al. (2015), ‘Diet dominates host genotype in shaping the murine gut microbiota.’, *Cell Host Microbe*, 17 (1), 72-84.
- 853**
- 854** Castoldi, Angela, et al. (2015), ‘They Must Hold Tight: Junction Proteins, Microbiota And Immunity In Intestinal Mucosa’, *Current Protein & Peptide Science*
- 855**
- 856** *Curr Protein Pept Sci*, 16 (7), 655-71.
- 857** Chang, Christopher C, et al. (2015), ‘Second-generation PLINK: rising to the challenge of larger and richer datasets’, *GigaScience*
- 858**
- 859** *GigaSci*, 4 (1), 7.
- 860** Chen, Congying, et al. (2018), ‘Contribution of Host Genetics to the Variation of Microbial Composition of Cecum Lumen and Feces in Pigs’, *Frontiers in Microbiology*
- 861**

- 862** *Front. Microbiol.*, 9
- 863** Chen, Haiwei, et al. (2019), 'A forward chemical genetic screen reveals gut microbiota metabolites that modulate host physiology', *Cell*, 177 (5), 1217-1231.e18.
- 864**
- 865** Chu, Hiutung and Sarkis K Mazmanian (2013), 'Innate immune recognition of the microbiota promotes host-microbial symbiosis', *Nat. Immunol.*, 14 (7), 668-75.
- 866**
- 867** Chung, HJ, et al. (2018), 'Gut Microbiota as a Missing Link Between Nutrients and Traits of Human.', *Front Microbiol*, 9
- 868** 1510.
- 869** Clapp, M, et al. (2017), 'Gut microbiota's effect on mental health: The gut-brain axis.', *Clin Pract*, 7 (4), 987.
- 870** Cohen, Louis J., et al. (2017), 'Commensal bacteria make GPCR ligands that mimic human signalling molecules', *Nature*, 549 (7670), 48-53.
- 871**
- 872** Cole, JR, et al. (2014), 'Ribosomal Database Project: data and tools for high throughput rRNA analysis.', *Nucleic Acids Res.*, 42 (Database issue), D633-42.
- 873**
- 874** Colosimo, Dominic A., et al. (2019), 'Mapping Interactions of Microbial Metabolites with Human G-Protein-Coupled Receptors', *Cell Host & Microbe*, 26 (2), 273-282.e7.
- 875**
- 876** Cox, Laura M. and Howard L. Weiner (2018), 'Microbiota Signaling Pathways that Influence Neurologic Disease', *Neurotherapeutics*, 15 (1), 135-45.
- 877**
- 878** Daniel, Noémie, Emelyne Lécuyer, and Benoit Chassaing (2021), 'Host/microbiota interactions in health and diseases—Time for mucosal microbiology', *Mucosal Immunology*, 1-11.
- 879**
- 880** Davenport, Emily R., et al. (2015), 'Genome-Wide Association Studies of the Human Gut Microbiota', *PLoS One*, 10 (11), e0140301.
- 881**
- 882** Davenport, Emily R. (2020), 'Genetic Variation Shapes Murine Gut Microbiota via Immunity', *Trends in Immunology*, 41 (1), 1-3.
- 883**
- 884** Deaver, Jessica A., Sung Y. Eum, and Michal Toborek (2018), 'Circadian Disruption Changes Gut Microbiome Taxa and Functional Gene Composition', *Frontiers in Microbiology*
- 885**
- 886** *Front Microbiol*, 9 737.
- 887** Delzenne, Nathalie M., et al. (2011), 'Targeting gut microbiota in obesity: effects of prebiotics and probiotics', *Nature Reviews. Endocrinology*
- 888**
- 889** *Nat Rev Endocrinol*, 7 (11), 639-46.
- 890** Doncheva, Nadezhda T., et al. (2019), 'Cytoscape StringApp: Network Analysis and Visualization of Proteomics Data', *Journal of Proteome Research*
- 891**
- 892** *J Proteome Res*, 18 (2), 623-32.
- 893** Erdman, S.E. and T. Poutahidis (2016), 'Microbes and Oxytocin', *131 (Int. Rev. Neurobiol., Elsevier)*, 91-126.
- 894** Fabian, Scheipl, Greven Sonja, and Kuechenhoff Helmut (2008), 'Size and power of tests for a zero random effect variance or polynomial regression in additive and linear mixed models.', *Computational Statistics & Data Analysis*, 52 (7), 3283-99.
- 895**
- 896**
- 897** Falconer, D. S (1996), *Introduction to quantitative genetics*, (Harlow, England: Prentice Hall).
- 898** Flux, M. C. and Christopher A. Lowry (2020), 'Finding intestinal fortitude: Integrating the microbiome into a holistic view of depression mechanisms, treatment, and resilience', *Neurobiology of Disease*
- 899**
- 900** *Microbiome in neurological and psychiatric disease*
- 901** *Neurobiology of Disease*, 135 104578.
- 902** Fonken, Laura K., et al. (2010), 'Light at night increases body mass by shifting the time of food intake', *Proceedings of the National Academy of Sciences*
- 903**
- 904** *PNAS*, 107 (43), 18664-69.
- 905** Foster, Jane A., Linda Rinaman, and John F. Cryan (2017), 'Stress & the gut-brain axis: Regulation by the microbiome', *Neurobiology of Stress*, 7 124-36.
- 906**
- 907** Fukata, Masayuki and Moshe Arditi (2013), 'The role of pattern recognition receptors in intestinal inflammation', *Mucosal immunology*, 6 (3), 451-63.
- 908**
- 909** Gastelum, C, et al. (2021), 'Adaptive Changes in the Central Control of Energy Homeostasis Occur in Response to Variations in Energy Status.', *Int J Mol Sci*, 22 (5), 2728.
- 910**
- 911** Gautam, D, et al. (2006), 'A critical role for beta cell M3 muscarinic acetylcholine receptors in regulating insulin release and blood glucose homeostasis in vivo.', *Cell Metab*, 3 (6), 449-61.
- 912**
- 913** Geraldles, A, et al. (2008), 'Inferring the history of speciation in house mice from autosomal, X-linked, Y-linked and mitochondrial genes.', *Mol Ecol*, 17 (24), 5349-63.
- 914**

- 915** Gevers, Dirk, et al. (2014), 'The treatment-naive microbiome in new-onset Crohn's disease', *Cell host & microbe*, 15 (3),
916 382-92.
- 917** Gogarten, Jan F, et al. (2021), 'Primate phageomes are structured by superhost phylogeny and environment', *Proceedings*
918 *of the National Academy of Sciences*, 118 (15),
- 919** Goodrich, Julia K., et al. (2014), 'Human genetics shape the gut microbiome', *Cell*, 159 (4), 789-99.
- 920** Goodrich, Julia K., et al. (2016), 'Genetic Determinants of the Gut Microbiome in UK Twins', *Cell host & microbe*,
- 921** Gould, AL, et al. (2018), 'Microbiome interactions shape host fitness.', *Proc. Natl. Acad. Sci. U S A*, 115 (51), E11951-60.
- 922** Gregory R. Warnes, Ben Bolker and Thomas Lumley (2020), 'gtools: Various R Programming Tools',
- 923** Grieneisen, L, et al. (2021), 'Gut microbiome heritability is nearly universal but environmentally contingent.', *Science*,
924 373 (6551), 181-86.
- 925** Groussin, Mathieu, et al. (2017), 'Unraveling the processes shaping mammalian gut microbiomes over evolutionary time',
926 *Nature Comm.*, 8 (1), 14319.
- 927** Hehemann, Jan-Hendrik, et al. (2010), 'Transfer of carbohydrate-active enzymes from marine bacteria to Japanese gut mi-
928 crobiota', *Nature*, 464 (7290), 908-12.
- 929** Hollander, Daniel and Jonathan D. Kaunitz (2020), 'The "Leaky Gut": Tight Junctions but Loose Associations', *Digestive*
930 *Diseases and Sciences*
- 931** *Dig Dis Sci*, 65 (5), 1277-87.
- 932** Hua, Yan, et al. (2020), 'Gut microbiota and fecal metabolites in captive and wild North China leopard (*Panthera pardus*
933 *japonensis*) by comparison using 16 s rRNA gene sequencing and LC/MS-based metabolomics', *BMC Veterinary Re-*
934 *search*, 16 (1),
- 935** Hughes, David A., et al. (2020), 'Genome-wide associations of human gut microbiome variation and implications for
936 causal inference analyses', *Nature Microbiology*, 5 (9), 1079-87.
- 937** Ishida, Sachiko, et al. (2020), 'Genome-wide association studies and heritability analysis reveal the involvement of host
938 genetics in the Japanese gut microbiota', *Communications Biology*
- 939** *Commun Biol*, 3
- 940** Kelly, John R., et al. (2015), 'Breaking Down the Barriers: The Gut Microbiome, Intestinal Permeability and Stress-relat-
941 ed Psychiatric Disorders', *Frontiers in Cellular Neuroscience*
- 942** *Front. Cell. Neurosci.*, 9
- 943** Kemis, Julia H., et al. (2019), 'Genetic determinants of gut microbiota composition and bile acid profiles in mice', *PLoS*
944 *Genet.*, 15 (8), e1008073.
- 945** Khan, Farhat, et al. (2021), 'IBDDB: a manually curated and text-mining-enhanced database of genes involved in inflam-
946 matory bowel disease', *Database*, 2021
- 947** Klug-Micu, GM, et al. (2013), 'CD40 ligand and interferon- γ induce an antimicrobial response against *Mycobacterium*
948 *tuberculosis* in human monocytes.', *Immunology*, 139 (1), 121-28.
- 949** Kohl, KD and MD Dearing (2014), 'Wild-caught rodents retain a majority of their natural gut microbiota upon entrance
950 into captivity.', *Environ Microbiol Rep*, 6 (2), 191-95.
- 951** Korach-Rechtman, H, et al. (2019), 'Murine Genetic Background Has a Stronger Impact on the Composition of the Gut
952 Microbiota than Maternal Inoculation or Exposure to Unlike Exogenous Microbiota.', *Appl. Environ. Microbiol.*, 85 (18),
953 e00826-19.
- 954** Kovacs, Amir, et al. (2011), 'Genotype is a stronger determinant than sex of the mouse gut microbiota', *Microbial ecolo-*
955 *gy*, 61 (2), 423-28.
- 956** Kurilshikov, Alexander, et al. (2021), 'Large-scale association analyses identify host factors influencing human gut micro-
957 biome composition', *Nat. Genet.*, 53 (2), 156-65.
- 958** Leamy, Larry J, et al. (2014), 'Host genetics and diet, but not immunoglobulin A expression, converge to shape composi-
959 tional features of the gut microbiome in an advanced intercross population of mice', *Genome Biology*
- 960** *Genome Biol*, 15 (12),
- 961** Ley, RE, et al. (2006), 'Microbial ecology: human gut microbes associated with obesity.', *Nature*, 444 (7122), 1022-23.
- 962** Li, J. and L. Ji (2005), 'Adjusting multiple testing in multilocus analyses using the eigenvalues of a correlation matrix',
963 *Heredity*, 95 (3), 221-27.
- 964** Lim, SJ and SR Bordenstein (2020), 'An introduction to phylosymbiosis.', *Proc Biol Sci*, 287 (1922), 20192900.
- 965** Linnenbrink, Miriam, et al. (2013), 'The role of biogeography in shaping diversity of the intestinal microbiota in house
966 mice', *Molecular Ecology*, 22 (7), 1904-16.
- 967** Lynch, SV and O Pedersen (2016), 'The Human Intestinal Microbiome in Health and Disease.', *N. Engl. J. Med.*, 375

- 968** (24), 2369-79.
- 969** Malaguarnera, L (2020), 'Vitamin D and microbiota: Two sides of the same coin in the immunomodulatory aspects.', *Int Immunopharmacol*, 79 106112.
- 970**
- 971** McKnite, Autumn M., et al. (2012), 'Murine Gut Microbiota Is Defined by Host Genetics and Modulates Variation of Metabolic Traits', *PLoS One*, 7 (6),
- 972**
- 973** McMurdie, Paul J and Susan Holmes (2013), 'phyloseq: an R package for reproducible interactive analysis and graphics of microbiome census data', *PLoS One*, 8 (4), e61217.
- 974**
- 975** Metwaly, Amira, et al. (2020), 'Integrated microbiota and metabolite profiles link Crohn's disease to sulfur metabolism', *Nature Comm.*, 11 (1),
- 976**
- 977** Walsh, Michael Lynch and Bruce (1998), *Genetics and Analysis of Quantitative Traits*, (Sunderland, MA: Sinauer).
- 978** Miller, Craig T., et al. (2014), 'Modular Skeletal Evolution in Sticklebacks Is Controlled by Additive and Clustered Quantitative Trait Loci', *Genetics*, 197 (1), 405-20.
- 979**
- 980** Mills, Robert H., et al. (2020), 'Organ-level protein networks as a reference for the host effects of the microbiome', *Genome Research*
- 981**
- 982** *Genome Res.*, 30 (2), 276-86.
- 983** Moeller, Andrew H., et al. (2016), 'Cospeciation of gut microbiota with hominids', *Science (New York, N.Y.)*
- 984** *Science*, 353 (6297), 380-82.
- 985** Moeller, Andrew H., et al. (2019), 'Experimental Evidence for Adaptation to Species-Specific Gut Microbiota in House Mice', *mSphere*, 4
- 986**
- 987** Moran, Nancy A. and Daniel B. Sloan (2015), 'The Hologenome Concept: Helpful or Hollow', *PLoS Biol.*, 13 (12), e1002311.
- 988**
- 989** Morgan, Andrew P., et al. (2015), 'The Mouse Universal Genotyping Array: From Substrains to Subspecies', *G3: GenesGenomesGenetics*
- 990** *G3 (Bethesda)*, 6 (2), 263-79.
- 991**
- 992** Moya, Andrés and Manuel Ferrer (2016), 'Functional Redundancy-Induced Stability of Gut Microbiota Subjected to Disturbance', *Trends Microbiol.*, 24 (5), 402-13.
- 993**
- 994** Nagpal, Ravinder, et al. (2020), 'Role of TRP Channels in Shaping the Gut Microbiome', *Pathogens*, 9
- 995** Neumann, Philipp-Alexander, et al. (2014), 'Gut Commensal Bacteria and Regional Wnt Gene Expression in the Proximal Versus Distal Colon', *The American Journal of Pathology*
- 996** *Am J Pathol*, 184 (3), 592-99.
- 997**
- 998** Nicholson, Jeremy K., et al. (2012), 'Host-gut microbiota metabolic interactions', *Science (New York, N.Y.)*
- 999** *Science*, 336 (6086), 1262-67.
- 1000** Nyholt, Dale R. (2019), 'matSpD local version - Statistical and Genomic Epidemiology Laboratory (SGEL)',
- 1001** O'Connor, Annalouise, et al. (2014), 'Responsiveness of cardiometabolic-related microbiota to diet is influenced by host genetics', *Mammalian Genome*, 25 (11), 583-99.
- 1002**
- 1003** Ochman, Howard, et al. (2010), 'Evolutionary relationships of wild hominids recapitulated by gut microbial communities', *PLoS Biol.*, 8 (11), e1000546.
- 1004**
- 1005** Org, Elin, et al. (2015), 'Genetic and environmental control of host-gut microbiota interactions', *Genome Research*
- 1006** *Genome Res.*, 25 (10), 1558-69.
- 1007** Org, Elin and Aldons J. Lusi (2018), 'Using the natural variation of mouse populations to understand host-gut microbiome interactions', *Drug discovery today: Disease models*
- 1008** *Drug Discov Today Dis Models*, 28 61-71.
- 1009**
- 1010** Ott, SJ, et al. (2004), 'Reduction in diversity of the colonic mucosa associated bacterial microflora in patients with active inflammatory bowel disease', *Gut*, 53 (5), 685-93.
- 1011**
- 1012** Pallares, LF, et al. (2014), 'Use of a natural hybrid zone for genomewide association mapping of craniofacial traits in the house mouse.', *Mol Ecol*, 23 5756-70.
- 1013**
- 1014** Pandey, Shubhi, Jagannath Maharana, and Arun K. Shukla (2019), 'The Gut Feeling: GPCRs Enlighten the Way', *Cell Host & Microbe*, 26 (2), 160-62.
- 1015**
- 1016** Papa, Eliseo, et al. (2012), 'Non-invasive mapping of the gastrointestinal microbiota identifies children with inflammatory bowel disease', *PLoS One*, 7 (6), e39242.
- 1017**
- 1018** Parker, Bianca J., et al. (2020), 'The Genus *Alistipes*: Gut Bacteria With Emerging Implications to Inflammation, Cancer, and Mental Health', *Frontiers in Immunology*
- 1019**

- 1020** *Front. Immunol.*, 11
- 1021** Parker, CC, et al. (2014), 'High-resolution genetic mapping of complex traits from a combined analysis of F2 and advanced intercross mice.', *Genetics*, 198 (1), 103-16.
- 1022**
- 1023** Peier, Andrea, et al. (2009), 'The Antiobesity Effects of Centrally Administered Neuromedin U and Neuromedin S Are Mediated Predominantly by the Neuromedin U Receptor 2 (NMUR2)', *Endocrinology*, 150 (7), 3101-9.
- 1024**
- 1025** Peng, Zhi, et al. (2020), 'The Gut Microbiome Is Associated with Clinical Response to Anti-PD-1/PD-L1 Immunotherapy in Gastrointestinal Cancer', *Cancer Immunology Research*
- 1026**
- 1027** *Cancer Immunol Res*, 8 (10), 1251-61.
- 1028** Qin, Junjie, et al. (2012), 'A metagenome-wide association study of gut microbiota in type 2 diabetes', *Nature*, 490 (7418), 55-60.
- 1029**
- 1030** Qin, Youwen, et al. (2020), 'Combined effects of host genetics and diet on human gut microbiota and incident disease in a single population cohort',
- 1031**
- 1032** Rapp, K (1972), 'HAN-rotation, a new system for rigorous outbreeding', *Z. Versuchstierk.*, 14 133-42.
- 1033** Rausch, P, et al. (2016), 'Analysis of factors contributing to variation in the C57BL/6J fecal microbiota across German animal facilities.', *Int. J. Med. Microbiol.*, 306 (5), 343-55.
- 1034**
- 1035** Rausch, Philipp, et al. (2019), 'Comparative analysis of amplicon and metagenomic sequencing methods reveals key features in the evolution of animal metaorganisms', *Microbiome*, 7 (1),
- 1036**
- 1037** Rehman, A, et al. (2016), 'Geographical patterns of the standing and active human gut microbiome in health and IBD.', *Gut*, 65 (2), 238-48.
- 1038**
- 1039** Reichardt, Nicole, et al. (2018), 'Specific substrate-driven changes in human faecal microbiota composition contrast with functional redundancy in short-chain fatty acid production', *The ISME Journal*, 12 (2), 610-22.
- 1040**
- 1041** Ricklin, D, et al. (2016), 'Complement component C3 - The "Swiss Army Knife" of innate immunity and host defense.', *Immunol. Rev.*, 274 (1), 33-58.
- 1042**
- 1043** Rieseberg, Loren H, Margaret A Archer, and Robert K Wayne (1999), 'Transgressive segregation, adaptation and speciation', *Heredity*, 83 (4), 363-72.
- 1044**
- 1045** Rolig, AS, et al. (2015), 'Individual Members of the Microbiota Disproportionately Modulate Host Innate Immune Responses.', *Cell Host Microbe*, 18 (5), 613-20.
- 1046**
- 1047** Rosshart, Stephan P., et al. (2017), 'Wild Mouse Gut Microbiota Promotes Host Fitness and Improves Disease Resistance', *Cell*, 171 (5), 1015-1028.e13.
- 1048**
- 1049** Roth, TL, et al. (2019), 'Reduced Gut Microbiome Diversity and Metabolome Differences in Rhinoceros Species at Risk for Iron Overload Disorder.', *Front Microbiol*, 10 2291.
- 1050**
- 1051** Rowland, Ian, et al. (2018), 'Gut microbiota functions: metabolism of nutrients and other food components', *European Journal of Nutrition*
- 1052**
- 1053** *Eur J Nutr*, 57 (1), 1-24.
- 1054** Rühlemann, Malte Christoph, et al. (2021), 'Genome-wide association study in 8,956 German individuals identifies influence of ABO histo-blood groups on gut microbiome', *Nat. Genet.*, 1-9.
- 1055**
- 1056** Saito, Yumiko, et al. (1999), 'Molecular characterization of the melanin-concentrating-hormone receptor', *Nature*, 400 (6741), 265-69.
- 1057**
- 1058** Sarkar, Amar, et al. (2020), 'The role of the microbiome in the neurobiology of social behaviour', *Biol. Rev.*, 95 (5), 1131-66.
- 1059**
- 1060** Sethi, JK and AJ Vidal-Puig (2008), 'Wnt signalling at the crossroads of nutritional regulation.', *Biochem. J.*, 416 (2), e11-3.
- 1061**
- 1062** Shannon, Paul, et al. (2003), 'Cytoscape: a software environment for integrated models of biomolecular interaction networks', *Genome Research*
- 1063**
- 1064** *Genome Res*, 13 (11), 2498-504.
- 1065** Shi, L and BP Tu (2015), 'Acetyl-CoA and the regulation of metabolism: mechanisms and consequences.', *Curr. Opin. Cell Biol.*, 33 125-31.
- 1066**
- 1067** Singh, Parul, et al. (2020), 'The potential role of vitamin D supplementation as a gut microbiota modifier in healthy individuals', *Scientific Reports*, 10 (1), 21641.
- 1068**
- 1069** Škrabar, N, et al. (2018), 'Using the *Mus musculus* hybrid zone to assess covariation and genetic architecture of limb bone lengths.', *Mol Ecol Resour*, 18 (4), 908-21.
- 1070**
- 1071** Smith, Ashley E., et al. (2019), 'Binge-Type Eating in Rats is Facilitated by Neuromedin U Receptor 2 in the Nucleus Accumbens and Ventral Tegmental Area', *Nutrients*, 11 (2), 327.
- 1072**
- 1073** Snijders, Antoine M., et al. (2016), 'Influence of early life exposure, host genetics and diet on the mouse gut microbiome

- 1074** and metabolome', *Nature Microbiology*, 2 16221.
- 1075** Spor, Aymé, Omry Koren, and Ruth Ley (2011), 'Unravelling the effects of the environment and host genotype on the gut
1076 microbiome', *Nature Reviews Microbiology*, 9 (4), 279-90.
- 1077** Sriram, K and PA Insel (2018), 'G Protein-Coupled Receptors as Targets for Approved Drugs: How Many Targets and
1078 How Many Drugs', *Mol. Pharmacol.*, 93 (4), 251-58.
- 1079** Steffen Durinck, Paul T. Spellman, Ewan
- 1080** Birney and Wolfgang Huber (2009), 'Mapping identifiers for the integration of genomic datasets with the
1081 R/Bioconductor package biomaRt.', *Nature Protocols*, 4 1184-91.
- 1082** Suzuki, TA (2017), 'Links between Natural Variation in the Microbiome and Host Fitness in Wild Mammals.', *Integr
1083* *Comp Biol*, 57 (4), 756-69.
- 1084** Suzuki, TA, et al. (2020), 'The gut microbiota and Bergmann's rule in wild house mice.', *Mol Ecol*, 29 (12), 2300-11.
- 1085** Suzuki, Taichi A and Ruth E Ley (2020), 'The role of the microbiota in human genetic adaptation', *Science*, 370 (6521),
- 1086** Suzuki, Taichi A., et al. (2019), 'Host genetic determinants of the gut microbiota of wild mice', *Molecular Ecology*, 28
1087 (13), 3197-207.
- 1088** Szklarczyk, Damian, et al. (2019), 'STRING v11: protein-protein association networks with increased coverage, support-
1089 ing functional discovery in genome-wide experimental datasets', *Nucleic Acids Research*
- 1090** *Nucleic Acids Res*, 47 (D1), D607-13.
- 1091** Tanahashi, Yasuyuki, et al. (2009), 'Multiple muscarinic pathways mediate the suppression of voltage-gated Ca²⁺
1092 channels in mouse intestinal smooth muscle cells', *Br. J. Pharmacol.*, 158 (8), 1874-83.
- 1093** Taras, David, et al. (2002), 'Reclassification of *Eubacterium formicigenerans* Holdeman and Moore 1974 as *Dorea formi-
1094* cigenans gen. nov., comb. nov., and description of *Dorea longicatena* sp. nov., isolated from human faeces.', *Internatio-
1095* *nal Journal of Systematic and Evolutionary Microbiology*, 52 (2), 423-28.
- 1096** Thaïss, Christoph A., et al. (2014), 'Transkingdom control of microbiota diurnal oscillations promotes metabolic home-
1097 ostasis', *Cell*, 159 (3), 514-29.
- 1098** Thaïss, Christoph A., Maayan Levy, and Eran Elinav (2015a), 'Chronobiomics: The Biological Clock as a New Principle
1099 in Host-Microbial Interactions', *PLoS Pathog.*, 11 (10), e1005113.
- 1100** Thaïss, Christoph A., et al. (2015b), 'A day in the life of the meta-organism: diurnal rhythms of the intestinal microbiome
1101 and its host', *Gut Microbes*, 6 (2), 137-42.
- 1102** Thaïss, Christoph A., et al. (2016), 'Microbiota Diurnal Rhythmicity Programs Host Transcriptome Oscillations', *Cell*,
1103 167 (6), 1495-1510.e12.
- 1104** Tian, Liang, et al. (2020), 'Deciphering functional redundancy in the human microbiome', *Nature Comm.*, 11 (1),
- 1105** Toderici, M, et al. (2016), 'Identification of Regulatory Mutations in SERPINC1 Affecting Vitamin D Response Elements
1106 Associated with Antithrombin Deficiency.', *PLoS One*, 11 (3), e0152159.
- 1107** Townsend, KL, et al. (2012), 'Bone morphogenetic protein 7 (BMP7) reverses obesity and regulates appetite through a
1108 central mTOR pathway.', *FASEB J.*, 26 (5), 2187-96.
- 1109** Turnbaugh, Peter J., et al. (2009), 'A core gut microbiome in obese and lean twins', *Nature*, 457 (7228), 480-84.
- 1110** Turnbaugh, PJ, et al. (2008), 'Diet-induced obesity is linked to marked but reversible alterations in the mouse distal gut
1111 microbiome.', *Cell Host Microbe*, 3 (4), 213-23.
- 1112** Turner, Leslie M., Denise J. Schwahn, and Bettina Harr (2012), 'Reduced Male Fertility Is Common but Highly Variable
1113 in Form and Severity in a Natural House Mouse Hybrid Zone', *Evolution*, 66 (2), 443-58.
- 1114** Turner, Leslie M. and Bettina Harr (2014), 'Genome-wide mapping in a house mouse hybrid zone reveals hybrid sterility
1115 loci and Dobzhansky-Muller interactions', *eLife*, 3 e02504.
- 1116** Turpin, W., et al. (2016), 'Association of host genome with intestinal microbial composition in a large healthy cohort',
1117 *Nat. Genet.*, 48 (11), 1413-17.
- 1118** Vaga, Stefania, et al. (2020), 'Compositional and functional differences of the mucosal microbiota along the intestine of
1119 healthy individuals', *Scientific Reports*, 10 (1),
- 1120** Valerie, Obenchain, et al. (2014), 'VariantAnnotation: a Bioconductor package for exploration and annotation of genetic
1121 variants', *Bioinformatics*, 30 (14), 2076-78.
- 1122** Velloso, Licio A., Franco Folli, and Mario J. Saad (2015), 'TLR4 at the Crossroads of Nutrients, Gut Microbiota, and
1123 Metabolic Inflammation', *Endocrine Reviews*
- 1124** *Endocr Rev*, 36 (3), 245-71.
- 1125** Wang, Jun, et al. (2015), 'Analysis of intestinal microbiota in hybrid house mice reveals evolutionary divergence in a ver-
1126 tebrate hologenome', *Nature Communications*

- 1127** *Nat Commun*, 6
- 1128** Wang, Jun, et al. (2016), 'Genome-wide association analysis identifies variation in vitamin D receptor and other host factors influencing the gut microbiota', *Nat. Genet.*, 48 (11), 1396-406.
- 1129**
- 1130** Wang, Y, et al. (2010), 'Regional mucosa-associated microbiota determine physiological expression of TLR2 and TLR4 in murine colon.', *PLoS One*, 5 (10), e13607.
- 1131**
- 1132** Weldon, L, et al. (2015), 'The Gut Microbiota of Wild Mice.', *PLoS One*, 10 (8), e0134643.
- 1133** Wu, Guangyan, et al. (2018), 'Light exposure influences the diurnal oscillation of gut microbiota in mice', *Biochemical and Biophysical Research Communications*
- 1134**
- 1135** *Biochem Biophys Res Commun*, 501 (1), 16-23.
- 1136** Yang, M, et al. (2020a), 'Mucosal-Associated Microbiota Other Than Luminal Microbiota Has a Close Relationship With Diarrhea-Predominant Irritable Bowel Syndrome.', *Front. Cell. Infect. Microbiol.*, 10 515614.
- 1137**
- 1138** Yang, Q, et al. (2020b), 'Role of Dietary Nutrients in the Modulation of Gut Microbiota: A Narrative Review.', *Nutrients*, 12 (2), E381.
- 1139**
- 1140** Yasuda, K, et al. (2021), 'Elucidation of metabolic pathways of 25-hydroxyvitamin D3 mediated by CYP24A1 and CYP3A using Cyp24a1 knockout rats generated by CRISPR/Cas9 system.', *J. Biol. Chem.*, 296 100668.
- 1141**
- 1142** Yatsunenka, Tanya, et al. (2012), 'Human gut microbiome viewed across age and geography', *Nature*, 486 (7402), 222-27.
- 1143**
- 1144** Yi, Z and GA Bishop (2015), 'Regulatory role of CD40 in obesity-induced insulin resistance.', *Adipocyte*, 4 (1), 65-69.
- 1145** Yu, Guangchuang, et al. (2012), 'clusterProfiler: an R package for comparing biological themes among gene clusters', *Omics: a journal of integrative biology*, 16 (5), 284-87.
- 1146**
- 1147** Zhou, Xiang and Matthew Stephens (2012), 'Genome-wide efficient mixed-model analysis for association studies', *Nat. Genet.*, 44 (7), 821-24.
- 1148**
- 1149** Ziyatdinov, Andrey, et al. (2018), 'lme4qtl: linear mixed models with flexible covariance structure for genetic studies of related individuals', *BMC Bioinformatics*, 19 (1), 1-5.
- 1150**